Articles

Transfer-NMR and Docking Studies Identify the Binding of the Peptide Derived from Activating Transcription Factor 4 to Protein Ubiquitin Ligase β-TrCP. Competition STD-NMR with β-Catenin†

Julien Pons,‡ Nathalie Evrard-Todeschi,‡ Gildas Bertho,‡ Josyane Gharbi-Benarous,‡ Valérie Tanchou,§ Richard Benarous,|| and Jean-Pierre Girault*,‡

Laboratoire de Chimie et Biochimie Pharmacologiques et Toxicologiques, Université Paris Descartes, UMR 8601 CNRS, 45 rue des Saint-Pères, 75270 Paris Cedex 06, France, Département des Maladies Infectieuses, Institut Cochin, Université Paris Descartes, U567-INSERM, UMR 8104 CNRS, Hôpital Cochin-Paris, Bat. G. Roussy, 27 rue du Faubourg St-Jacques, 75014 Paris, France, and CEA ValRhô, Direction des Sciences du Vivant, Institut de Biologie Environnementale et Biotechnologie, Service de Biochimie et Toxicologie Nucléaire, BP1717, 30207 Bagnols sur Cèze, France

Received July 19, 2007; Revised Manuscript Received September 27, 2007

ABSTRACT: ATF4 plays a crucial role in the cellular response to stress. The E3 ubiquitin ligase, SCF β-TrCP protein responsible for ATF4 degradation by the proteasome, binds to ATF4 through a DpSG*XXX*pS phosphorylation motif, which is similar but not identical to the DpSG*XX*pS motif found in most other substrates of β-TrCP. NMR studies were performed on the free and bound forms of a peptide derived from this ATF4 motif that enabled the elucidation of the conformation of the ligand complexed to the β-TrCP protein and its binding mode. Saturation transfer difference (STD) NMR allowed the study of competition for binding to β-TrCP, between the phosphorylation motifs of ATF4 and β-catenin, to characterize the ATF4 binding epitope. Docking protocols were performed using the crystal structure of the β-catenin−β-TrCP complex as a template and NMR results of the ATF4−β-TrCP complex. In agreement with the STD results, in order to bind to β-TrCP, the ATF4 DpSGIXXpSXE motif required the association of two negatively charged areas, in addition to the hydrophobic interaction in the β-TrCP central channel. Docking studies showed that the ATF4 DpSGI*XX*pS*X*E motif fits the binding pocket of β-TrCP through an S-turning conformation. The distance between the two phosphate groups is 17.8 Å, which matched the corresponding distance 17.1 Å for the other extended DpSG*XX*pS motif in the β-TrCP receptor model. This study identifies the residues of the β-TrCP receptor involved in ligand recognition. Using a new concept of STD competition experiment, we show that ATF4 competes and inhibits binding of β-catenin to β-TrCP.

ATF4[1] (Figure 1A) is a member of the ATF/CREB b-ZIP transcription factors that bind to DNA by their basic region and dimerize *via* their leucine zipper domain to form a large variety of homodimers and/or heterodimers that allows the cell to coordinate signals from different pathways (Figure 2) (*1*, *2*). ATF4 plays a crucial role in response to various cellular stress conditions like ER stress, heme deficiency, amino acid deprivation, viral infections and dsRNA expression (Figure 2). Multiple intracellular stress pathways (*3*) converge on a single event, phosphorylation of eIF2α, which leads both to a general inhibition of protein synthesis and also to the translational up-regulation of the mRNA encoding ATF4 (*4*−*7*). Thus the targets of ATF4 are of paramount importance in a generalized stress response. In addition, ATF4 is important for cell proliferation and differentiation (*8*, *9*). ATF4 is a critical regulator of osteoblast differentiation and function (*10*) and of bone resorption (*11*). ATF4 is also

† This work was supported by grants from the Sidaction and ANRS Associations.

* Address correspondence to this author. Tel: 33-1-42-86-21-80. Fax: 33-1-42-86-83-87. E-mail: jean-pierre.girault@univ-paris5.fr.

‡ Laboratoire de Chimie et Biochimie Pharmacologiques et Toxicologiques, Université Paris Descartes.

§ CEA ValRhô, Direction des Sciences du Vivant, Institut de Biologie Environnementale et Biotechnologie, Service de Biochimie et Toxicologie Nucléaire.

|| Département des Maladies Infectieuses, Institut Cochin, Université Paris Descartes.

[1] Abbreviations: AARE, amino acid-response element; ATF4, activating transcription factor 4; β-Cat, β-catenin; β-TrCP, transducin repeat-containing protein; b-ZIP, the basic region and the leucine zipper domain; Cul1, Cullin 1; TSP-d_4, 3-(trimethylsilyl)[2,2,3,3-d_4]-propionic acid, sodium salt; HSQC, heteronuclear single quantum correlation; IκBα, inhibitor of nuclear factor kappa B alpha; MBP, maltose binding protein; NOE, nuclear Overhauser effect; NFκB, nuclear factor kappa B; NOESY, nuclear Overhauser effect spectroscopy; P-, phosphorylated peptide; pS, phosphorylated serine; PBS, phosphate-buffered saline; SCF, Skp1/Cul1/F-box; Skp1, suppressor of kinetochore protein; STD-NMR, saturation-transfer difference NMR spectroscopy; TOCSY, total correlation spectroscopy; TPPI, time proportional phase incrementation; TRNOESY, transferred nuclear Overhauser effect spectroscopy; ROESY, rotating-frame Overhauser enhancement spectroscopy; TNE, Tris NaCl EDTA; Vpu, HIV-1 encoded virus protein U; WATERGATE, water suppression by gradient-tailored excitation.

10.1021/bi7014212 CCC: $40.75
Published on Web 12/05/2007

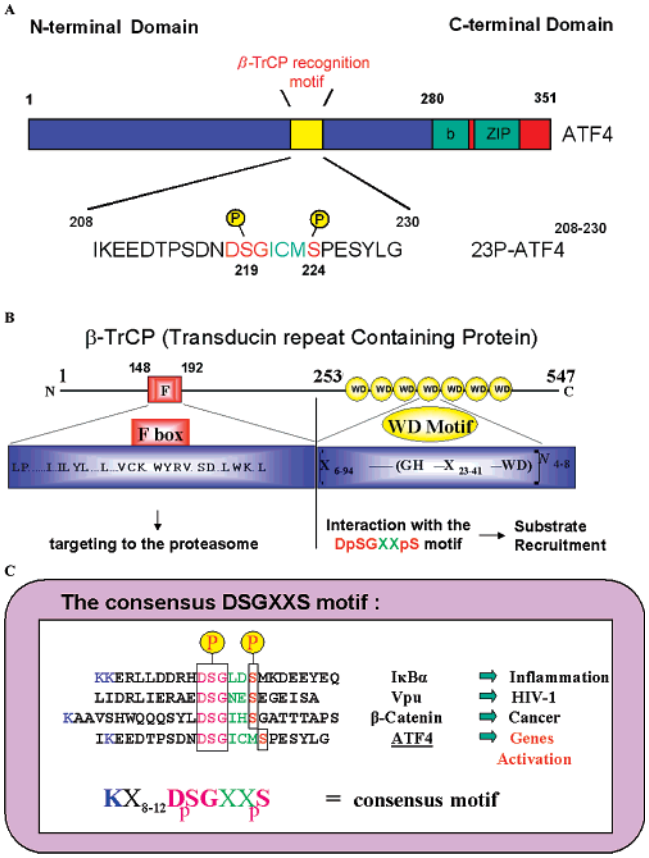

FIGURE 1: Scheme of protein structures of β-TrCP and ATF4. (A) Schematic representation of the ATF4 structure. The basic region and the leucine zipper domain (b-ZIP) are indicated in addition to the DSG*XXX*S motif. Interaction of β-TrCP with ATF4 is impaired by mutation on the Asp[218] and Ser[219] ATF4 residues. (B) The diagram of β-TrCP shows the F box responsible for proteasome targeting through Skp1 binding and the seven WD40 repeats involved in binding substrates. (C) The phosphorylation site containing the consensus motif D**pS**G*XX***pS** is shown in four peptide ligands of the β-TrCP protein.

involved in long-term memory induction (*12*). Hence, ATF4 is a master transcription factor for which temporal expression and activity are under tight cellular control (Figure 2) (*13*−*15*).

ATF4 represents a novel substrate for the SCF−β-TrCP complex (Figure 1B), which is the first mammalian E3 ubiquitin ligase identified so far for the control of the degradation of a b-ZIP transcription factor. The F-box protein β-TrCP (Figure 1B), the receptor component of the SCF E3 ubiquitin ligase, is colocalized in the nucleus with ATF4 and controls its stability (*16*) and subsequently its transcriptional activity. Association between the two proteins depends on ATF4 phosphorylation and on ATF4 serine residue 219 present in the context of D**pS**G*XXX***pS**, which is similar but not identical to the motif found in other substrates of β-TrCP (Figure 1C).

The domain responsible for substrate binding activity of β-TrCP is the seven WD40 repeats (named β-propeller) at the C terminus-recognition domain (Figure 1B). The protein−protein interactions involved can be mimicked by a short phosphorylated peptide including the degradation motif D**pS**G$X_{(2-4)}$**pS**. The three-dimensional structure of the human β-TrCP−Skp1 complex bound to a β-catenin peptide had been determined by X-ray crystallography (*17*). NMR studies

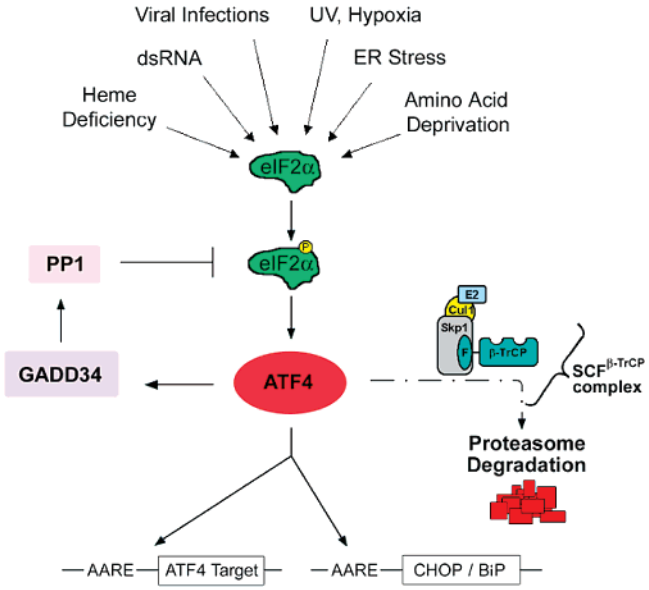

FIGURE 2: Schematic illustration of ATF4 activation via eIF2α phosphorylation. Protein kinases, PKR, HRI, PERK and GCN2 are activated by multiple intracellular stress pathways (viral infections, heme deficiency, endoplasmic reticulum stress, hypoxia, amino acid starvation and exposure to oxidant or reactive metals) and converge on a single event, phosphorylation of eIF2α, which allows the expression of the ATF4 transcription factor that in turn induces GADD34 transcription (*58*). Transcriptional induction of GADD34 results in the activation of PP1 and the dephosphorylation of eIF2α after prolonged exposure to hypoxia. Finally, the ATF4 and eIF2α pathways converge to optimally induce targets that include CHOP and BiP. Thus the targets of ATF4 are of paramount importance in a generalized stress response. Lassot et al. showed that $SCF^{\beta TrCP}$ tightly modulates the stability of the transcription factor ATF4 and therefore also modulates its transcriptional activity following activation of the cAMP pathway (*16*, *58*).

Table 1: Sequence of the β-TrCP Peptide Ligands[a]

name	sequence number	sequence	source
23P-ATF4	208−230	IKEEDTPSDN**DSGICMS**-PESYLG	NMR[b]
24P-IκBα	21−44	KKERLLDDRH**DSGLDS**-MKDEEYEQ	NMR[b]
22P-Vpu	41−62	LIDRLIERAE**DSGNES**-EGEISA	NMR[b]
32P-β-catenin	17−48	DRKAAVSHWQQQSYL**DSGI-HS**GATTTAPSLSG	NMR[b]
11P-β-catenin	30−40	YL**DSGIHS**GAT	X-ray

[a] Sequence of five peptide ligands of the β-TrCP protein. Structures used for binding mode prediction. [b] NMR, minimized average structure.

utilizing transfer NOE techniques complemented the crystallographic studies and identified the conformation of several β-TrCP ligands (Table 1) including Vpu, IκBα, and β-catenin (*18*−*20*). They share the canonical phosphorylated motif, D**pS**G*XX***pS**, required for interaction with β-TrCP. However, several other substrates of β-TrCP that do not harbor the canonical D**pS**G*XX***pS** motif, including ATF4, have recently been identified.

In the present work, we studied by NMR techniques the binding to β-TrCP of ATF4 using two peptides of 23 amino acids referred to ATF4 fragment (208−230), 23-ATF4 and 23P-ATF4 for the phosphorylated peptide at the two sites Ser[219] and Ser[224]. NMR techniques were used to assess the particular influence of the presence of an additional residue

between the two serine residues in the binding motif. Transferred nuclear Overhauser enhancement (TRNOE) spectroscopy (*21*, *22*) completed by molecular modeling is successfully applied to investigate the conformation of a ligand in its bound form. Utilizing saturation transfer difference NMR (STD-NMR) techniques, a model for the binding epitope of 23P-ATF4 peptide bound to β-TrCP was derived. Here, experimental data that complement the structural β-TrCP complex data collected to date are presented. STD-NMR has been established as an important technique to identify binding activities and to characterize binding epitopes of ligands with atomic resolution (*23*−*25*). Docking ATF4 ligand starting from NMR bound conformer is essential to predict ATF4 ligand binding mode and to consider β-TrCP protein structural variations in ligand binding as only NMR bound structure determined in solution is available for the target. Molecular docking therefore plays an important role in structure-based drug design (*26*, *27*).

Since numerous substrates sharing related but not identical phosphorylation motif have recently been identified, we wanted to address the important question of the competition between substrates for the binding to β-TrCP. Toward this goal we performed a competition STD-NMR method, which extends the STD-NMR with competitive binding and allows the detection of the higher affinity ligand in the ATF4−β-catenin mixture for the same binding site. This method can also derive a lower limit for the dissociation constant of ATF4 ligand (*28*). This STD-NMR method can rapidly be extended to rank order analogues and derive structure−activity relationships.

1. MATERIALS AND METHODS

1.1. Peptide Synthesis. ATF4 fragment (208−230) hereafter referred to as peptides 23P-ATF4 and 23-ATF4 was purchased from NeoMPS Lab., Strasbourg (France). The amino acid sequence is I^{208}KEEDTPSDND**pS**GICM-**pS**PESYLG^{230} for the peptide (derived from the human protein) containing the phosphorylated sites 219 and 224, Ser(PO_3H_2). The peptide nonphosphorylated at Ser^{219} and Ser^{224} was used as a reference. The two peptides were *N*-acylated and *C*-amidated at their respective termini. The purity (95%) of the peptides was tested by analytical HPLC and by mass spectrometry.

1.2. Purification of the WD Repeat Region from Human Protein β-TrCP Fused to the Maltose Binding Protein (MBP). Coding sequence corresponding to the 253−547 residues of full-length protein β-TrCP was inserted into the pMAL-C2X expression vector (OZYME). The construction resulted in a fusion protein of approximately 75 kDa corresponding to the 361 residues of the MBP (*29*), a 33-mer linker and the seven WD repeats (residues 253−547) of β-TrCP hereafter named MBP-β-TrCP. Saturated overnight preculture of *Escherichia coli* Rosetta transformed with pMAL-C2X::TrCP WD was diluted 1:200 in Luria broth medium (LB) containing 50 mg/L ampicillin, 20 mg/L chloramphenicol and 2 g/L (D+)-glucose monohydrate (Sigma-Aldrich), and allowed to grow until $OD_{600nm} = 0.5$ at 37 °C. Protein expression was induced at 30 °C for 4 h with 1 mM isopropyl-β-D-thiogalactopyranoside (IPTG). After centrifugation at 4000 rpm for 20 min at 4 °C, the pellet was washed in pH 7.2 TNE buffer (20 mM Tris, 200 mM NaCl, 1 mM EDTA) containing a protease inhibitor cocktail (ROCHE). The solution was then disrupted at 0.9 kbar, centrifuged at 20000*g* for 45 min at 4 °C and the supernatant containing soluble proteins was recovered. Amylose Resin (New England BioLabs) was pre-equilibrated in TNE and added to the supernatant to allow the binding for 1 h at room temperature, with gentle shaking. The beads were then washed three times with TNE to remove nonspecific binding. MBP-β-TrCP was eluted by competition with TNE containing 10 mM maltose for 30 min at room temperature. Proteins were analyzed on a NuPAGE 4−12% Bis-Tris gel (Invitrogen) and coomassie staining. Protein concentration was determined using the standard Bradford method following the OD at 595 nm. At last, the purified recombinant protein was concentrated using Amicon Ultra-15 centrifugal filter units (Millipore) with a 10 kDa molecular weight cutoff and dialyzed in NMR buffer in order to remove maltose. Following this protocol, the final yield of purified MBP-β-TrCP was of 3.5 mg/L. This amount of purified recombinant protein was used to prepare the NMR samples.

1.3. NMR Spectroscopy. The experiments were run at 500.13 MHz for ^1H on Bruker AVANCE 500 spectrometer with a Linux PC workstation, using sample tubes with a 5-mm outer diameter. Two-dimensional NMR spectra were recorded in the phase-sensitive mode using the States-TPPI method (*30*) for quadrature detection in the t_1 dimension. All experiments were carried out using the WATERGATE pulse sequence for water suppression (*31*) or using the excitation sculpting water suppression (*32*) to eliminate solvent signal in $H_2O/^2H_2O$ 95:5 solution. The following conventional two-dimensional experiments TOCSY (*33*), NOESY (*34*), and ROESY (*35*) spectra were recorded at several temperatures within the 280−310 K range. TOCSY spectra were recorded using a MLEV-17 spin−lock sequence (*36*) with a mixing time (τ_m) of 35 and 70 ms, respectively. For 2D NOESY experiments an optimal mixing time of 300 ms was observed in the 50−500 ms range. For 2D ROESY experiments, a spin−lock of 50−400 ms was used. Two-dimensional ^1H, ^1H spectra were acquired with 256 t_1 increments, 4096 data points, and a relaxation delay of 2 s, spanning a spectral width of 11.0 ppm. Spectra were acquired with 32 scans/t_1 increment for NOESY and ROESY, 8 scans/t_1 increment for TOCSY. Spectra were processed using XWIN-NMR 3.5 (Bruker). For the 2D heteronuclear experiments, $^1H-^{13}C$ HSQC (*37*), $^1H-^{13}C$ HSQC with multiplicity editing during selection step (*38*) and $^1H-^{13}C$ HMBC (*39*) performed in aqueous solution, water resonance was suppressed with low-power presaturation. The spectra were recorded with 512(t_1) × 4096(t_2) data points and with a proton spectral width of 5482.5 Hz in water and a carbon spectral width of 21380.6 Hz. Spectra were analyzed with FELIX (Accelrys) software, and chemical shift assignments were done manually (Tables 2and 3), using data from TOCSY, NOESY, HMBC and HSQC experiments.

1.3.1. NMR Spectroscopy of Ligand−Protein Interaction. The spectra of the free peptides at 2 mM sample concentration were recorded at 280 K in 50 mM sodium phosphate buffer at pH 7.2, prepared in 95% H_2O and 5% ^2H_2O. The NMR sample of peptide in the presence of β-TrCP contained 20 μM protein and 2 mM peptide, for a ratio of 100:1 peptide:protein binding sites, in PBS solution, 50 mM (NaH_2PO_4/Na_2HPO_4), pH 7.2, containing 0.02% NaN_3 and 5% ^2H_2O. In order to avoid the oxidation of cysteine, it is

Table 2: Proton Chemical Shift Assignments[a]

residues			NH	CαH	Cβ H	other
	CH_3CO	(CH_3CO)		2.03		
1	Ile	(I208)	8.31	4.11	1.82	Cγ$_1$H 1.48/1.19; Cγ$_2$H 0.91; CδH 0.90
2	Lys	(K209)	8.60	4.38	1.83/1.77	CγH 1.43; CδH 1.69; CϵH 3.00
3	Glu	(E210)	8.76	4.26	2.06/1.95	CγH 2.30
4	Glu	(E211)	8.70	4.29	2.09/1.94	CγH 2.29
5	Asp	(D212)	8.53	4.65	2.71/2.62	
6	Thr	(T213)	8.31	4.60	4.13	CγH 1.27
7	Pro	(P214)		4.39	2.33/1.93	CγH 2.05; CδH 3.86/3.84
8	Ser	(S215)	8.70	4.47	3.90	
9	Asp	(D216)	8.57	4.64	2.71/2.63	
10	Asn	(N217)	8.52	4.73	2.84/2.73	NγH 7.84/7.05
11	Asp	(D218)	8.47	4.66	2.76/2.68	
12	pSer	(S219)	9.01	4.46	4.10/4.07	
13	Gly	(G220)	8.63	4.02/3.91		
14	Ile	(I221)	7.97	4.18	1.88	Cγ$_1$H 1.48/1.18; Cγ$_2$H 0.91; CδH 0.89
15	Cys	(C222)	8.69	4.51	2.89	
16	Met	(M223)	8.72	4.58	2.11/2.00	CγH 2.63/2.55; CϵH 2.08
17	pSer	(S224)	8.90	4.82	4.10/4.08	
18	Pro	(P225)		4.47	2.35/1.96	CγH 2.06; CδH 3.87/3.90
19	Glu	(E226)	8.79	4.19	2.02/2.12	CγH 2.30
20	Ser	(S227)	8.28	4.39	3.85	
21	Tyr	(Y228)	8.31	4.59	3.06	Ar2.6H 7.15 ; Ar3.5H 6.83
22	Leu	(L229)	8.27	4.25	1.58	CγH 1.46; CδH 0.91
23	Gly	(G230)	7.92	3.87/3.83		
	$CONH_2$	($CONH_2$)	7.23/7.46			

[a] ^{1}H NMR chemical shifts of the mixture of 2 mM 23P-ATF4 peptide and 0.02 mM MBP-β-TrCP protein in ppm from TSP-d_4. Spectra were recorded at 280 K, pH 7.2, 23P-ATF4/β-TrCP = 100 (2 mM 23P-ATF4 peptide, 0.02 mM MBP-β-TrCP protein) and 50 mM sodium phosphate buffer; H_2O:^2H_2O, 95:5 (by volume). The chemical shifts observed are the averages of those of the bound peptide and the peptide excess.

Table 3: ^{13}C NMR Chemical Shifts Assignments[a]

residues			^{13}C′	^{13}Cα	^{13}Cβ	other
	CH_3CO	(CH_3CO)	176.9		21.4	
1	Ile	(I208)	176.6	58.4	35.8	Cγ 24.4; Cδ 14.5
2	Lys	(K209)	176.3	53.1	30.2	Cγ 21.6; Cδ 26.1; Cϵ 39.2
3	Glu	(E210)	176.2	54.0	27.3	Cγ 33.3
4	Glu	(E211)	176.7	53.6	27.3	Cγ 33.2
5	Asp	(D212)	175.9	51.6	38.2	
6	Thr	(T213)	176.1	57.0	66.8	Cγ 18.5
7	Pro	(P214)	*b*	61.2	29.2	Cγ 24.6; Cδ 60.9
8	Ser	(S215)	175.7	55.3	61.2	
9	Asp	(D216)	174.1	51.5	38.2	
10	Asn	(N217)	175.6	50.3	36.3	Cγ 177.0
11	Asp	(D218)	174.7	51.5	38.3	
12	pSer	(S219)	176.1	55.4	61.9	
13	Gly	(G220)	174.9	42.6		
14	Ile	(I221)	173.8	58.2	35.8	Cγ 24.4; Cδ 14.6
15	Cys	(C222)	176.1	55.7	24.8	
16	Met	(M223)	176.3	56.9	30.3	Cγ 29.0
17	pSer	(S224)	174.9	53.2	62.7	
18	Pro	(P225)	*b*	60.4	29.4	Cγ 24.5; Cδ 61.1
19	Glu	(E226)	177.4	54.5	27.4	Cγ 33.5
20	Ser	(S227)	175.5	56.1	61.1	
21	Tyr	(Y228)	174.4	55.5	35.6	Cδ 130.4; Cϵ 115.4
22	Leu	(L229)	175.9	52.5	39.0	Cγ 23.7; Cδ 22.1
23	Gly	(G230)	177.3	42.1		
	$CONH_2$	($CONH_2$)	176.6			

[a] ^{13}C NMR chemical shifts of the mixture of 2 mM 23P-ATF4 peptide and 0.02 mM MBP-β-TrCP protein in ppm from TSP-d_4. Spectra were recorded at 280 K, pH 7.2, 23P-ATF4/β-TrCP = 100 (2 mM 23P-ATF4 peptide, 0.02 mM MBP-β-TrCP protein) and 50 mM sodium phosphate buffer; H_2O:^2H_2O, 95:5 (by volume). The chemical shifts observed are the averages of those of the bound peptide and the peptide excess. [b] Not determined.

recommended to degas solvents well in order to remove oxygen present. Moreover, it is preferable to avoid the basic mediums to solubilize peptide and then to quickly use it after its setting in solution.

The one-dimensional STD-NMR (*24*, *25*) spectrum of β-TrCP/peptide was performed at 500 MHz and 280 K with 1024 scans (or 10 240 for a better signal-to-noise ratio) and a relaxation delay of 2.0 s. STD spectra were recorded with selective saturation of protein resonances with *on-resonance* irradiation at 11 ppm or −1 ppm and *off-resonance* irradiation at 30 ppm for reference spectra. A series of 40 Gaussian shaped pulses (50 ms with 1 ms delay between pulses, $\gamma B_1/2 = 110$ Hz) were used, for a total saturation time of 2.04 s. The 1D STD spectra were obtained by internal subtraction of saturated spectra from reference spectra by phase cycling.

Transferred nuclear Overhauser effect (TRNOESY) (*22*) spectra of β-TrCP/peptide were recorded at 500 MHz and 280 K. The observed TRNOE correlations were large and negative; a sample of the nonphosphorylated peptide in the presence of the protein showed only minimal NOE intensities with a mixing time of 150 ms. Structure calculations were based on a spectrum recorded with a mixing time of 150 ms. Automatic baseline correction was performed prior to integration of cross-peak volumes using FELIX (Accelrys). Cross-peak intensities were converted to distances (*40*) by using the distance between the Tyr^{228} H aromatic protons (2.43 Å) as a reference. The TRNOE cross−peak intensities were classified as strong (1.8−2.7 Å), medium (1.8−3.6 Å) and weak (1.8−5.0 Å).

1.3.2. Titration WaterLOGSY To Evaluate the K_d. Titration WaterLOGSY permits, after proper correction, the evaluation of the dissociation binding constant. The details of the pulse sequence version used for the WaterLOGSY experiment reported here can be found in the literature (*41*). The first water selective 180° pulse does not require high selectivity, and, in our experiment, a pulse of 20 ms length was found to be sufficient. The first two pulsed field gradients (PFGs) have a typical length of 2 ms and a power strength of 4.4 G/cm. This strength is sufficient to destroy the unwanted magnetization, and, at the same time, it avoids signal losses due to diffusion occurring between the first two PFGs. A

weak rectangular PFG is applied during the entire length of the mixing time. A short gradient recovery time of 1 ms is applied at the end of the mixing time before the detection pulse. The water suppression in both experiments was achieved with the excitation sculpting sequence (*32*). The two water selective 180° square pulses and the four PFGs of the scheme were 2.7 ms. The data were collected with a sweep width of 6009.62 Hz, an acquisition time of 1.363 s, and a relaxation delay of 0.5 s. Prior to Fourier transformation the data were multiplied with an exponential function with a line broadening of 1 Hz.

1.3.3. STD Binding Competition Experiment. A competition STD-NMR experiment allows the detection of the higher affinity ligand indirectly by monitoring the STD signals of β-catenin ligand in the ATF4−β-catenin mixture on β-TrCP protein (*28*). The STD experiments can be used in a qualitative way to detect if the known X-ray ligand (β-catenin) is displaced in the presence of other NMR substrates thus, regarded as inhibitors. This is demonstrated with 1D STD-NMR spectra of a mixture composed of the β-catenin−β-TrCP complex in the absence and in the presence of the 23P-ATF4 peptide (100:0, 70:30, 50:50 and 30:70, respectively).

1.4. Three-Dimensional Structure Calculation. The calculated distances were incorporated into ARIA 1.2 simulated annealing protocol running within the program CNS (*42*, *43*) for molecular dynamics calculations using the PARALLHDG 5.3 force field. During the calculations, non-glycine residues were restrained to negative ϕ values (usually the only range considered in NMR-derived structures) (*44*). ARIA enabled the incorporation of ambiguous distance restraints and calibration of the NOE restraints using automated matrix analysis as implemented by the program (*45*). ARIA runs were performed using the default parameters with eight iterations. In the final iteration, a set of lowest-energy structures was retained as the final structures. The set of peptide structures was selected for correct geometry and no distance restraint violations of >0.5 Å. Analysis of the structures was performed within AQUA, PROCHECK-NMR (*46*) programs. MOLMOL (*47*) and LITHIUM 2.1 (Tripos) were used for the analysis and presentation of the results of the structure determination. Finally, 10 structures were chosen to represent the conformation of the peptide that is consistent with NMR data. An average structure was taken as a representative structure.

1.5. Docking of the NMR Structure. We studied the docking of 23P-ATF4 ligand molecule into β-TrCP protein binding site. Surflex-Dock 2.0 (SYBYL 7.3) docks flexible ligands into a rigid receptor (*48*). Surflex-Dock docking program uses an empirical scoring function to dock ATF4 active ligand into β-TrCP protein binding site determined by X-ray crystallography (*17*). In the first docking stage, we validated the docking process, starting from structure initially derived from the complex β-TrCP protein bound to a ligand β-catenin peptide, a cocrystallized molecule (PDB ID code 1P22). The protein structure consists of the three-dimensional structure of the human β-TrCP−Skp1 complex. To examine the possible mechanism of action of the ATF4 ligand on the β-TrCP receptor, we replaced β-catenin by ATF4 NMR conformations in the β-TrCP binding site. The peptide was taken in its putative (NMR) binding conformations, and was superimposed to β-catenin in the X-ray model.

Docking is guided by the protomol an idealized representation of the intended binding site in which putative ligands make every potential interaction (electrostatic, hydrophobic, hydrogen bonds...). The protomol can be defined from on a known active site, here, the seven WD repeats of β-TrCP: residues 253−547. The ligand is extracted into a separate molecule area. Consisting of molecular probes (CH_4, C═O, N−H), the protomol is a representation of the receptor binding cavity to which putative ligands are aligned. Two parameters determine the extent of the protomol: (i) Threshold value is a factor determining how much the protomol can be buried in the protein and increasing this number will decrease the volume. (ii) Bloat value can be used to inflate the protomol and include nearby crevices. The threshold and bloat values were optimized to 0.3 and 1, respectively. The specified ligand includes hydrogen atoms and is provided in NMR conformation to evaluate the experimental interaction between the ligand and the receptor. After completion of an interactive docking run, the docked ligand appears and Surflex-Dock produced 30 conformations of the ligand into the active site. They are listed in descending order of score values expressed as $-\log(K_d)$. The conformation with the highest score is displayed. The scoring function includes the following terms: hydrophobic, polar, repulsive, entropic and solvation to represent binding affinities. The docked ligand was compared to the experimental NMR structures. The ATF4 ligand was docked successfully.

2. RESULTS

2.1. NMR Resonance Assignments. ^{1}H chemical shifts and resonance assignments were established using two-dimensional ^{1}H, ^{1}H TOCSY, NOESY, and ROESY experiments. The ^{13}Cα signals were assigned using ^{13}C-edited HSQC (*38*) and HMBC (*39*) experiments on a ^{13}C natural abundance sample. Chemical shifts at 280 K and at pH 7.2 were reported in Table 2 (^{1}H) and Table 3 (^{13}C) for the 23P-ATF4 peptide in the presence of the MBP-β-TrCP protein. Sequential assignments of ^{1}H resonances were based on characteristic sequential NOE connectivities observed between the α-proton of residue i and the amide proton of residue $i + 1$, i.e., $d\alpha N(i, i + 1)$, in both NOESY and ROESY data sets. The ambiguities in the assignment were resolved using sequential $C^{\alpha}H-NH(i, i + 1)$ connectivities in the NOESY spectrum. A NOE cross-peak was observed between the CαH of Ser^{224} and CδH of Pro^{225} and similarly, between the CαH of Thr^{213} and CδH of Pro^{214} suggesting the X-Pro bond to be mainly *trans* (*49*). The NMR spectra of the peptides revealed that the peptides exist in two isoforms due to *cis*-*trans* isomerization about the Ser^{224}−Pro^{225} amide bond. A NOE between Ser^{224} Hα and Pro^{225} Hα, characteristic of *cis*-proline, was apparent and confirmed the presence of a *cis*/*trans* isomer mixture. The ratio of *trans* to *cis* isomer was estimated to be 7:3, based on the differential signal intensity of the resolved indole NH resonance of each isomer in the one-dimensional ^{1}H spectrum. No *cis*−*trans* isomerization was detected across the Thr^{213}−Pro^{214} amide bond, but this does not exclude the possibility that a small amount of the peptide, too small to be detected by NMR, exhibits the *cis* configuration.

Thus, the NMR data reveal that the major species of peptide 23P-ATF4 is the *trans* isomer.

2.2. Determination of β-TrCP−Peptide Equilibrium Constants K_d. The dissociation constant was measured by NMR

for the interaction of the phosphorylated 23P-ATF4 peptide to the MBP-β-TrCP protein. WaterLOGSY represents a powerful method for primary NMR screening in the identification of compounds interacting with macromolecules. Several relay pathways are used in the experiment for transferring bulk water magnetization to the ligand. The method is particularly useful for the evaluation of the dissociation binding constant (*28*). Titration WaterLOGSY can be recorded to extract, after proper correction, the evaluation of the K_d. The WaterLOGSY signals for the ligand in the presence of the protein can then be corrected by subtracting the value of the ligand signals recorded in the absence of the protein. The resulting corrected data are now lying on a dose response curve (Figure S1 of Supporting Information) and, assuming a simple binding mechanism, the data can be fitted to the equation

$$I = \frac{-I_{max}}{1 + \frac{L}{K_D}} + I_{max} \quad (1)$$

where I_{max} is the maximum WaterLOGSY signal and L the free ligand concentration. The dissociation binding constant K_d measured with eq 1 is characteristic of fast exchange condition, 23P-ATF4, $K_d = 500$ μM, 32P-β-catenin, $K_d = 1000$ μM, 22P-Vpu, $K_d = 200$ μM, 24P-IκBα, $K_d = 400$ μM, at 280 K. This range of binding affinity made the peptide likely to be suitable for TRNOESY NMR experiments, which require fast exchange between the free and bound states.

2.3. Interaction of 23P-ATF4 with β-TrCP. To investigate the interaction of the 23P-ATF4 peptide, with β-TrCP, we performed STD (*23*−*25*, *50*, *51*) and TRNOE (*21*, *22*) NMR experiments.

The STD-NMR technique is a method of epitope mapping by NMR spectroscopy. During the experiment, resonances of the protein are selectively saturated, intramolecular NOEs develop within the protein and, in addition, they give rise to intermolecular NOE effects in a binding ligand. These negative NOE effects may be observed as enhancements in the difference (STD-NMR) spectrum resulting from subtraction of this spectrum from a reference spectrum in which the protein is not saturated (Figure 3). Enhancements are observed for the resonance of protons in close contact with the protein, and this allows direct observation of areas of the ligand that comprise the epitope (*23*−*25*, *50*, *51*). The individual signal protons of the 23P-ATF4 peptide are analyzed from the intensity values in the reference (I_0) and STD spectra ($I_{STD} = I_0 - I_{sat}$). The spectral region corresponding to the amino protons is well resolved and can be used to classify the amino acid residues relevant for interaction with the protein (Figure 3B). Figures 3A,B shows *in black* the 1D STD-NMR spectrum of the alkyl and the amide protons, respectively, and *in red* a normal ^{1}H-spectrum of the complex of 23P-ATF4 with the protein. The signal obtained with the largest I_{STD}/I_0 value, the **pSer**^{219} H−N proton, was normalized to 100% (Figure 3C). The relative degree of saturation for the individual protons, normalized to that of **pSer**^{219}, can be used to compare the STD effect (*24*). The STD-NMR spectra show clearly that H−N resonances of the ^{218}D**pS**GICM**pS**^{224} motif and the **Glu**^{226} residue have STD intensities between 70 and 100% (Figure 3C). Obviously, these residues have more and tighter contacts with the protein surface. In addition, enhancements (50−70%) of the amide resonances of Lys^{209}−Asp^{212} and Ser^{215}−Asn^{217} were apparent, indicating that these residues are involved in the epitope. The lowest intensities (<50%) are found for both end-residues, the N-terminal (Ile^{208}) and the C-terminal (Gly^{230}) groups, along with Thr^{213} and Tyr^{228} residues. Thus, a clear distinction between protons with a strong contact to the protein and the others can be made. No enhancements of resonances of the minor *cis* isomer were observed.

For reference, the STD-NMR spectrum was recorded with a sample containing the nonphosphorylated 23-ATF4 peptide in the presence of the MBP-β-TrCP protein. This provided a negative control (Figure S2D of Supporting Information). In this case, the STD spectrum does not contain ligand signals. No effects can be observed as enhancements of the signals of protons, because of the absence of contact between 23-ATF4 and the β-TrCP protein. Thus, saturation transfer does not occur without the Asp-**pSer**-Gly-*XXX*-**pSer** motif. This showed that the large number of the enhancements observed for the 23P-ATF4 peptide in the presence of the MBP-β-TrCP protein (Figure S2A) was caused by the areas of the ligand actually in contact with the β-TrCP binding site. Another STD-NMR experiment of control was performed with phosphorylated 23P-ATF4 peptide and MBP fusion protein, lacking the seven WD domain of β-TrCP protein. The control samples were prepared under conditions similar to those used for the 23P-ATF4/MBP-β-TrCP sample. The resulting one-dimensional spectrum contained no signals (Figure S2B), demonstrating the specificity of the interaction observed between 23P-ATF4 and the MBP-β-TrCP fusion protein (Figure S2A). Another experimental way to distinguish here between specific effects of binding peptide to its target and nonspecific interactions between ligand and macromolecular complex was to use in control experiments, the ligand alone (Figure S2C). In that case, STD spectra using an on-resonance of −1 ppm did not contain ligand signals, showing that saturation transfer via the protein was the sole reason for the effects observed using samples with the ligand molecules in the presence of MBP-β-TrCP (Figure S2A).

The combination of STD-NMR epitope mapping data with knowledge of the bound conformation of ligands, which may be obtained by TRNOESY experiments, is a powerful method to build up models of protein−ligand interaction (*52*−*54*). Therefore, TRNOESY experiments (*21*, *22*) were used to investigate the bound conformation of the peptide. The optimal conditions for the TRNOESY measurements were determined by considering a peptide:β-TrCP molar ratio of 100 with mixing times (τ_m) of 50, 100, 150, 300 and 500 ms. After a NOE buildup analysis (Figure 4A) (*55*), a mixing time of 150 ms was used for the peptide in the presence of β-TrCP. At the 150 ms mixing time there is no spin diffusion in the TRNOESY. The free peptide showed very poor NOESY spectra at this mixing time, only sequential NOEs; the inter-residue NOEs could be observed at mixing times higher that 150 ms, when we increased the mixing time to 500 ms. To regard the spin-diffusion effect, we conducted a TRROESY with the mixing time of 100 ms for direct comparison with TRNOESY at 150 ms, so as to check the validity of the observed TRNOEs. Inter-residue ^{1}H−^{1}H distances deduced from ROE and NOE volumes are in

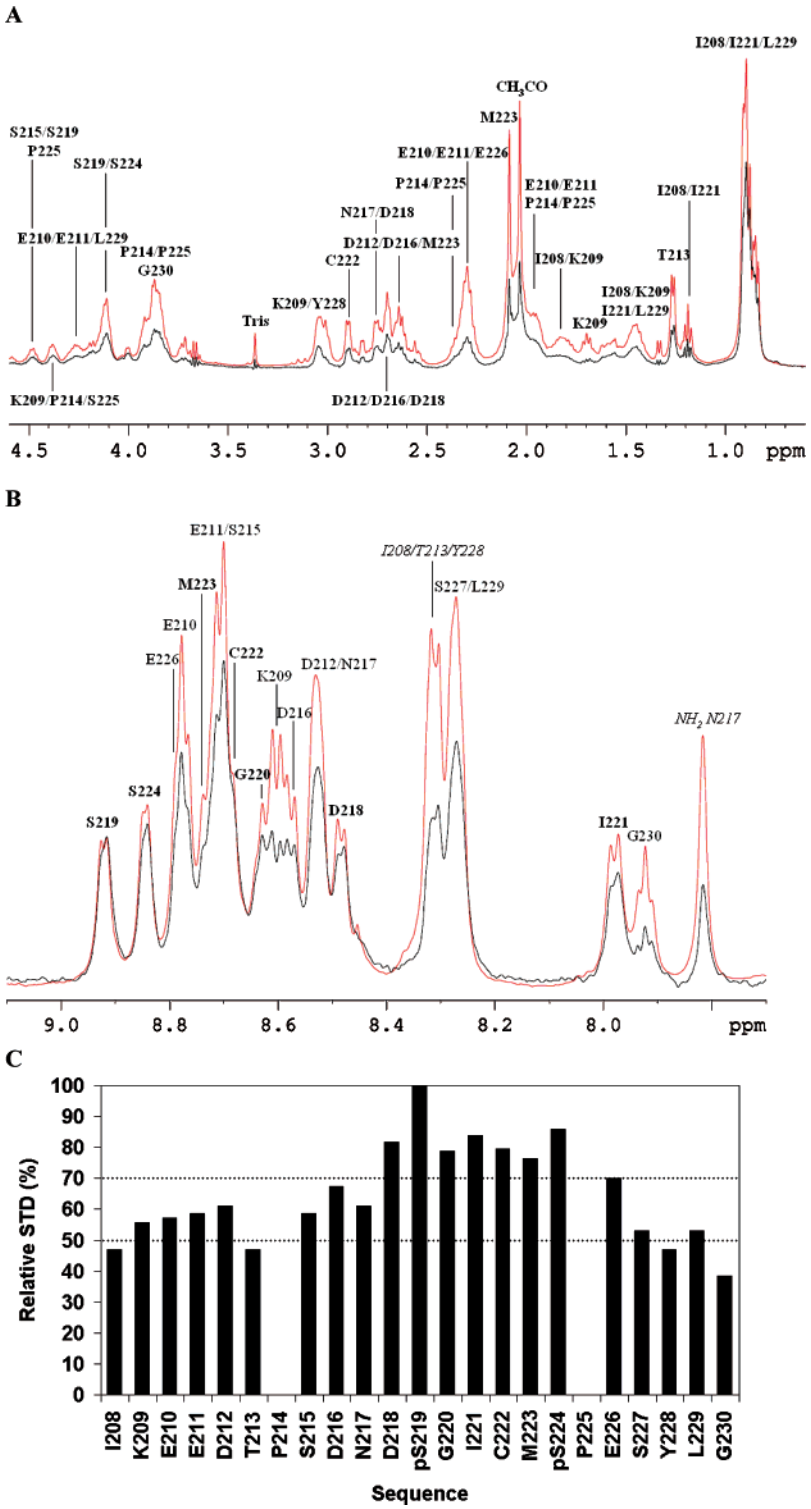

FIGURE 3: (A) Expansion of the region containing resonances of the alkyl protons of the 23P-ATF4 peptide in association with the β-TrCP protein and (B) expansion of the region containing resonances of the amide protons of the 23P-ATF4 peptide in association with the β-TrCP protein. Reference 1D ^{1}H spectrum (in red) and 1D ^{1}H STD-NMR spectrum (in black), showing enhancements of resonances of protons making close contacts with protein interaction site. STD spectra were recorded with selective saturation of protein resonances with *on-resonance* irradiation at −1 and 11 ppm and *off-resonance* irradiation at 30 ppm for reference spectra (a series of 40 Gaussian shaped pulses were used, for a total saturation time of 2.04 s). STD values are obtained after peak picking intensities compared to the 1D with the exact values of chemical shifts of the HN (in bold, amino acids with intense relative STD, and in italic, amino acids with weak relative STD). The signal at 7.8 ppm is low in intensity: the side chain of the residue Asn217 has a weak contact to the protein surface. (C) Relative STD intensities for 23P-ATF4 peptide. The integral value of the largest signal of the 23P-ATF4 peptide, the **pSer**^{219} HN proton, was set to 100%. The relative degree of saturation for the individual protons normalized to that of the **pSer**^{219} can be used to compare the STD effect (*24*). The relative intensities have been classified arbitrarily in three categories (dashed lines).

agreement. The 2D ROESY spectra were recorded with a mixing time of 100 ms and 64 scans for each of the 512 t_1 increments using a spin−lock field of $\gamma B_1 = 1190$ Hz at 5.0 ppm. It is usually assumed that TRROESY can be interpreted on the assumption that, at least for short mixing times, spin-diffusion effects can be ignored. Nevertheless, the use of

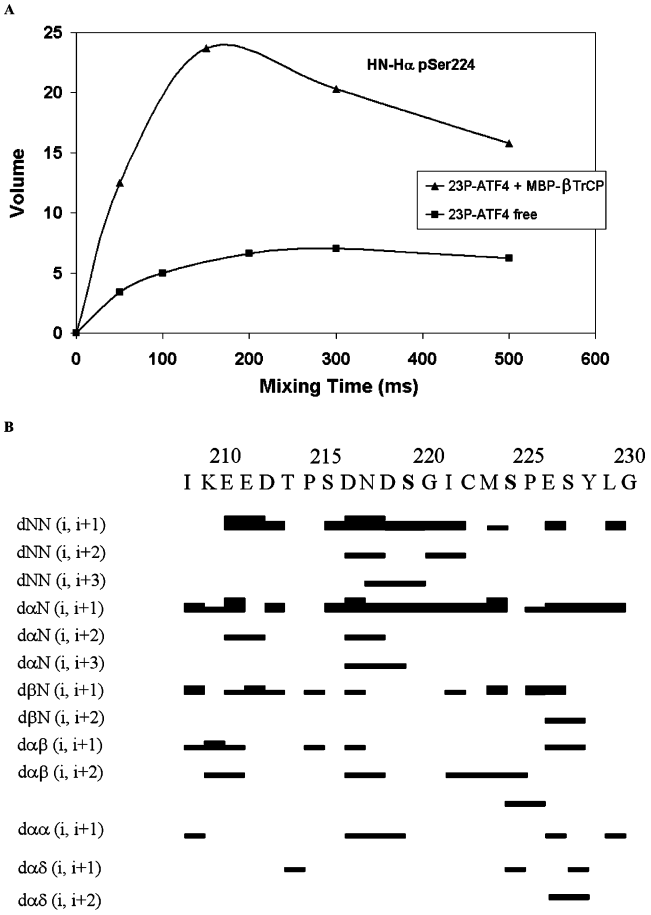

FIGURE 4: (A) NOE build-up rates of 23P-ATF4 peptide with or without β-TrCP protein vs mixing time (ms). The ligand to β-TrCP protein ratio is 100:1. The curves represent the intra-residue connectivity HN/Hα of **pSer**^{224}. (B) Sequential $d(i, i + 1)$, and medium range $d(i, i + 2)$, and $d(i, i + 3)$ ^{1}H$-^1$H TRNOE connectivities in the 23P-ATF4 peptide (sequence at the top) in the presence of the β-TrCP protein at 280 K and pH 7.2. The thickness of the lines reflects the relative intensities of the NOEs within the individual plots.

TRROESY to test spin diffusion can be limited, and when it was possible, a good approach to exploit nuclear Overhauser effects to determine internuclear distances between pairs of protons, without perturbation of spin-diffusion effects should be the QUIET-TRNOESY NMR experiment (*56*). The TRNOEs observed for the 23P-ATF4 peptide are summarized in Figure 4B. The turnlike structure was well-defined particularly in the region of Ser^{215} to **pSer**^{224}, where a loop (Ileu$^{221}-$Tyr^{228}) consecutive to a first turn (Ser$^{215}-$Ile^{221}) was apparent (Figure 5). Inter-residue contacts (Table S1 and Figure S3 of Supporting Information) such as dNN$(i, i + 2)$, $d\alpha$N$(i, i + 2)$ and $d\alpha\beta(i, i + 2)$ between Asp^{216} and Asp^{218}, dNN$(i, i + 2)$ between Gly^{220} and Cys^{222}, dNN$(i, i + 3)$ between Asn^{217} and Gly^{220}, and $d\alpha$N$(i, i + 3)$ between Asp^{216} and pSer^{219}, helped to define the first turn part (Ser$^{215}-$Ile^{221}) of the large bend. Strong contact $(i, i + 1)$, $d\alpha$N from Cys^{222} to Leu^{229}, $d\beta$N from Met^{223} to Ser^{227}, $d\alpha\beta$ between Glu^{226} and Ser^{227} and other inter-residue contacts such as $(i, i + 2)$, $d\beta$N between Glu^{226} and Tyr^{228} and $d\alpha\beta$ between pSer^{224} and Glu^{226}, characterized the second part (Ileu$^{221}-$Tyr^{228}) of this hairpin loop structure (Figure 5B).

TRNOE experiments led to 316 distant restraints (Table 4) incorporated for structure calculation. The structural statistics for the ten lowest energy structures (Figure 5A), generated by ARIA in the final iteration, are shown in Table 4. The average root-mean-square difference (rmsd) for superimposition of the 10 bound structures with lowest NOE restraint energy (Figure 5A), with the lowest energy structure as a template (Figure 5B), was 1.9 ± 0.6 Å for the backbone atoms (N, Cα, C′, O), but for the 219−224 region, this value decreased to 0.5 ± 0.2 Å (Table 4). This is confirmed by the plot of the rmsd of the backbone dihedral ϕ and ψ angles values for the family of the 10 structures of the 23P-ATF4 bound peptide (Figure S4 of Supporting Information). The graphic highlights the well-ordered part of the peptide (210−227). Interestingly, it corresponds to the residues that were shown to be the most involved in the binding surface as evidenced in the STD-NMR experiments (Figure 5C). The calculated structures (Figure 5 and Table 4) comprise a large bend with two opposite loops, Ser$^{215}-$Ile^{221} and Ile$^{221}-$Ser^{227}, respectively. In the calculated conformation, an intramolecular **pSer**^{219} O′−Ile^{221} HN hydrogen bond was present. This structure would expose the Ileu^{221} in the center and the two phosphorylated Ser (**pSer**^{219} and **pSer**^{224}) side chains implemented in the bend (Ser$^{215}-$Ser^{227}) for interactions with the β-TrCP protein (Figure 5C), a hypothesis consistent with the STD-NMR data (Figure 5C).

2.4. Docking of ATF4 Peptide. As described in Materials and Methods, ligand flexibility was treated by pregenerating the 23P-ATF4 bound peptide with the ARIA software and then docking the bound ligand conformer into the protein target as a rigid molecule. The energy scores of the conformers were then merged for the ligand. The conformer with the highest score represented the docked ligand. Redocking 11P-β-catenin (Figures 6A,B) into its cocrystallized protein structure (β-TrCP) referred to as native docking was successful (dock score 5.1 and rmsd = 2.37 Å). This docking (Figure 6E) will serve as a validation of the docking algorithm and the scoring function used in ATF4 study. Figure 6F shows that single docking correctly identified the near-native binding mode when the 11P-β-catenin ligand was redocked to its cocrystallized β-TrCP protein structure. For comparison, Figures 6C and 6D display the binding mode of 11P-β-catenin observed in the crystal structure. The phosphoserine, aspartic acid, and hydrophobic residues of the motif are recognized directly by contacts from β-TrCP (Figure 6D). The best-scored conformation will be useful for further analysis.

Different ligands induce different binding mode prediction. Figure 7A shows the result of β-TrCP−receptor docking against the NMR minimized structure of the bound 23P-ATF4 peptide. The 23P-ATF4 ligand, *via* the bound NMR energy-minimized structure, was cross-docked into the β-TrCP crystal structure originally bound with another ligand (11P-β-catenin). The 23P-ATF4 ligand structures were superimposed by matching 15 backbone atoms in the binding site (the D**pS**GIC fragment). Figure 7 shows the best-scored conformation of the ATF4 ligand after different docking runs. The conformer with the highest score (dock score 5.1) represented the docked ligand, and the docking accuracy was evaluated in terms of the rmsd between the docking model and the experimentally NMR bound structure (rmsd = 3.7 Å). Table S2 lists the database rmsd fitting of the ten

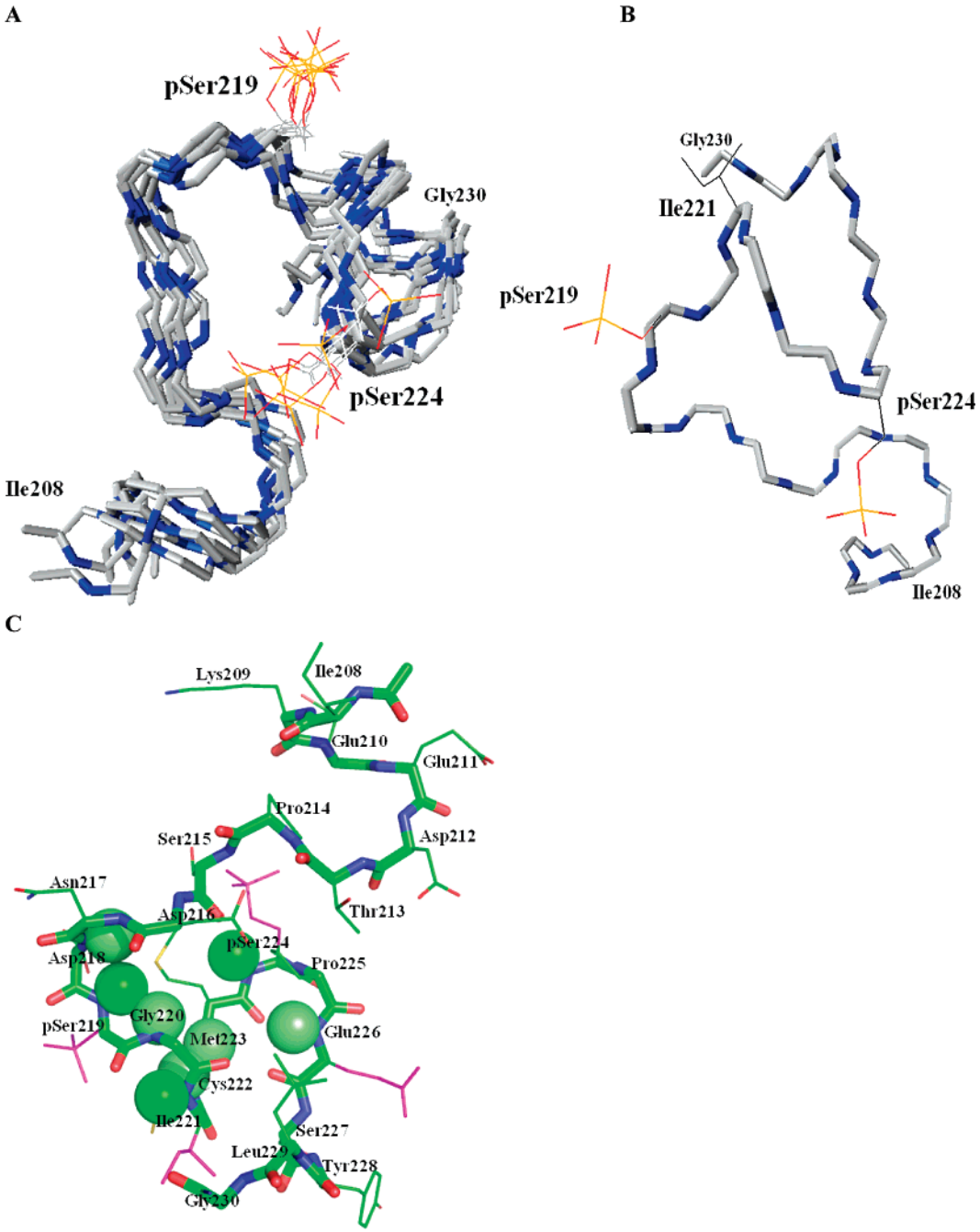

FIGURE 5: TRNOE derived structure of the bound 23P-ATF4 peptide. (A) 10 structures were generated with ARIA, and the structures are displayed bound to β-TrCP. Superimposition from residue 215 to residue 230. (B) A representative structure of 23P-ATF4 bound to β-TrCP. (C) Amide protons with the strongest STD amplification factor are displayed as colored spheres: green for the strongest, Ileu^{221}, **pSer**^{219} and **pSer**^{224}; light green for Asp^{218}, Gly^{220}, Cys^{222}, Met^{223} and Glu^{226}. The motif forms a large bend with two opposite loops. This structure exposes the Ileu^{221} in the center and the two phosphorylated **pSer**^{219}, **pSer**^{224} and Glu^{226} side chains implemented in the bend for interactions with the β-TrCP protein.

conformers with the highest score. They represented ensemble docking of the NMR structure.

As shown in Figure 7B docking using the NMR structure identified the binding mode of the ligand. The NMR 23P-ATF4 bound structure docks near amino acids known to be in the interaction site (β-catenin−β-TrCP complex) on the surface of the β-TrCP protein. Interestingly, the docking results highlight the binding of the D**pS**G**I***XX***pS***X***E** motif (Figure 7C) shown to play a significant role in the stabilization of the complex, particularly the **pSer**^{219}, **pSer**^{224}, **Ile**^{221} and the **Glu**^{226} residues. On the other hand, the STD results (Figure 3C) show strong enhancements, ranging from 70% to 100%, for amide protons of similar ^{218}D**pS**G**I**CM**pS***X***E**^{226} motif, indicating that these residues are also involved in the epitope binding (Figure 7C).

The contacts between ATF4 and β-TrCP involve essentially the first strand that lines the central channel (Figure 6A). The ATF4 with acidic residues docks near amino acids known to be in the interaction site (Tyr^{271}, Arg^{285}, Ser^{309}, Ser^{325}, Arg^{410}, Arg^{431}, Gly^{432} and Ser^{448}) on the top face of the WD domain of the protein β-TrCP. They are essentially attached through hydrogen bonds. (Figure 7B).

2.5. STD ATF4/β-Catenin β-TrCP Binding Competition Experiment. The ability to detect the higher-affinity ligand

Table 4: Structural Statistics of the Final 20 NMR Structures of the 23P-ATF4 Bound to the β-TrCP Protein

no. of exptl distance restraints	
unambiguous NOE	224
ambiguous NOE	92
total NOEs	316
divided into	
intraresidue NOE	150
sequential NOE	113
medium range NOE	40
long-range NOE	13
no. of exptl broad dihedral restraints	20
NOE violations >0.3 Å per structure	0.4
rmsd[a] (Å) to a mean molecule	
backbone (all residues)	1.9 ± 0.6
heavy atoms (all residues)	2.7 ± 0.7
backbone (residues 215−230)	1.7 ± 0.6
heavy atoms (residues 215−230)	2.5 ± 0.6
backbone (residues 207−219)	1.3 ± 0.6
heavy atoms (residues 207−219)	2.2 ± 0.6
backbone (residues 219−224)	0.5 ± 0.2
heavy atoms (residues 219−224)	1.5 ± 0.4
Ramachandran plot of residues[b] (%)	
in most favored regions	38.9
in additional allowed regions	55.6
in generously allowed regions	5.6
in disallowed regions	0.0

[a] Calculated by MOLMOL. [b] Calculated by PROCHECK.

by the competition STD-NMR method was applied using STD signals resulting from 23P-ATF4, and 32P-β-catenin when a mixture of different concentrations of these peptides were mixed in the presence of the β-TrCP protein. This experiment was made possible because the STD signals obtained upon binding ATF4 and β-catenin to β-TrCP are clearly different, which allows the simultaneous detection of these signals when both peptides are mixed. As shown in Figure 8, a significant reduction and disappearance of the STD signals of the β-catenin ligand in the presence of increasing amount of the ATF4 peptide proved the ability of the higher affinity ATF4 ligand to successfully compete with the lower affinity β-catenin ligand for the same binding site on β-TrCP. The weak β-catenin ligand ($K_D \approx 1000\ \mu$M) at a concentration of 0.4 mM in the presence of 0.02 mM β-TrCP shows STD signals of the amide protons, essentially of the first phosphorylated serine, **pSer**^{33}, and the aromatic protons NϵH of Trp^{25} (Figure 8A). 32P-β-catenin was selected as the STD indicator. Figures 8B−D display the 1D STD-NMR spectra of a mixture composed of 32P-β-catenin and 23P-ATF4 70:30, 50:50 and 30:70, respectively, with β-TrCP. A substantial reduction in the STD signal intensities of 32P-β-catenin **pSer**^{33} and Trp^{25} was observed, which indicated the presence of an active ligand in the mixture. At the first addition of ATF4 (70:30), the **pSer**^{219}, **pSer**^{224} signals appeared at 9.05 and 8.90 ppm, identifying 23P-ATF4 as a ligand (Figure 8B).

Figure 8 illustrates the reduction of the STD signal of the STD indicator (32P-β-catenin) according to the concentration of the competitor (23P-ATF4). As shown in Figure 8, the signal corresponding to the first serine **pSer**^{33} and Trp^{25} (β-catenin) decreased in the presence of increasing concentration of ATF4. Proton signal at 9.42 ppm corresponding to the second one, **pSer**^{37}, strongly decreased and disappeared completely in the STD spectra, indicating that this residue is not involved any more in the interaction. This is in agreement with the stronger binding signal given by the first **pSer** residue compared to the second upon binding for all substrates to β-TrCP. Adding of the same amount (0.4 mM) of 23P-ATF4 (50:50) inhibits the binding of 32P-β-catenin, and compared to the STD effect of 32P-β-catenin before ATF4 was added, the signal of the protons **pSer**^{33} NH decreased by 20%, approximately (Figure 8C). For instance, to achieve a 50% STD signal reduction of 32P-β-catenin, a concentration of 1 mM (30:70) is required for 23P-ATF4 (Figure 8D). NMR spectra gave strong STD effects of the 23P-ATF4 (0.2 mM) binding peptide which was present in the solution at 100-fold excess to the β-TrCP protein (0.02 mM). At this excess, the protein is occupied by the stronger ligand (23P-ATF4), and as a consequence 32P-β-catenin signals do not show up in the STD spectrum due to a loss in intensity.

The competition STD-NMR method led to specific ATF4 binding to β-TrCP, to competition with β-catenin and to identification of inhibitor of β-catenin-β-TrCP interaction. Finally, the dissociation constant of 23P-ATF4 was estimated to be 500 μM, which agrees well with the value evaluated by WaterLOGSY (*28*).

3. DISCUSSION

Deletion experiments allowed the mapping of the interacting domains between the two β-TrCP and ATF4 proteins, respectively, on the seven WD40 repeats at the C terminus of β-TrCP and between residues 87 to 279 of ATF4 (*16*). The seven WD40 repeats (W1−W7) form a toruslike structure (named β-propeller) that is characteristic of the β-TrCP, which presents a narrow channel running through the middle of the toruslike structure (Figure 6A).

3.1. Comparison of the Docked Peptide Structure to the NMR Structure. The ATF4 conserved structures from NMR and docking share a common structural organization with a central bend including the two turn regions involved in interaction of the peptide ligand (Figure 9). The NMR bound conformer is required to preposition favorably the peptide. The comparison between Figure 9A and Figure 9B shows that the NMR conformer correctly reflects this ligand-induced fit effect. The binding motif forms an S-turn structure in ATF4, from NMR (Figure 9A) and docking (Figure 9B), whereas the shorter motif adopts an extended conformation in β-catenin (Figure 9C).

It was interesting to observe the structural similarities of the docked fragment and the corresponding NMR bound conformation. In the two structures, the binding motif was represented by a similar large bend ND**pS**G**I***XX***pS***X***E** (interatomic distance between the two carbonyl atoms, Asn^{217}CO−Glu^{226}CO 18.5 Å in the docked structure; 18.2 Å in the bound structure). The bend was characterized by Ile^{221} in the center of a first turn in the ND**pS** region, and a second turn due to **pS***X***E** residues. Each of both loops was characterized by similar interatomic distance: Ile^{221}Cβ−**pSer**^{219}P (9.5 Å in the docked structure; 8.5 Å in the NMR bound structure) for the first loop, and Ile^{221}Cβ−**pSer**^{224}P (13.3 Å in the docked structure; 14.0 Å in the bound structure) for the second one. The resemblance of the two structures was also found in an equivalent measurement of the extreme distances from the two loops: Asn^{217}CO−Ileu^{221}Cβ (12.1 Å in the docked structure; 12.7 Å in the bound structure), and Ileu^{221}Cβ−Glu^{226}CO (10.3 Å in the docked structure; 10.2 Å in the bound structure).

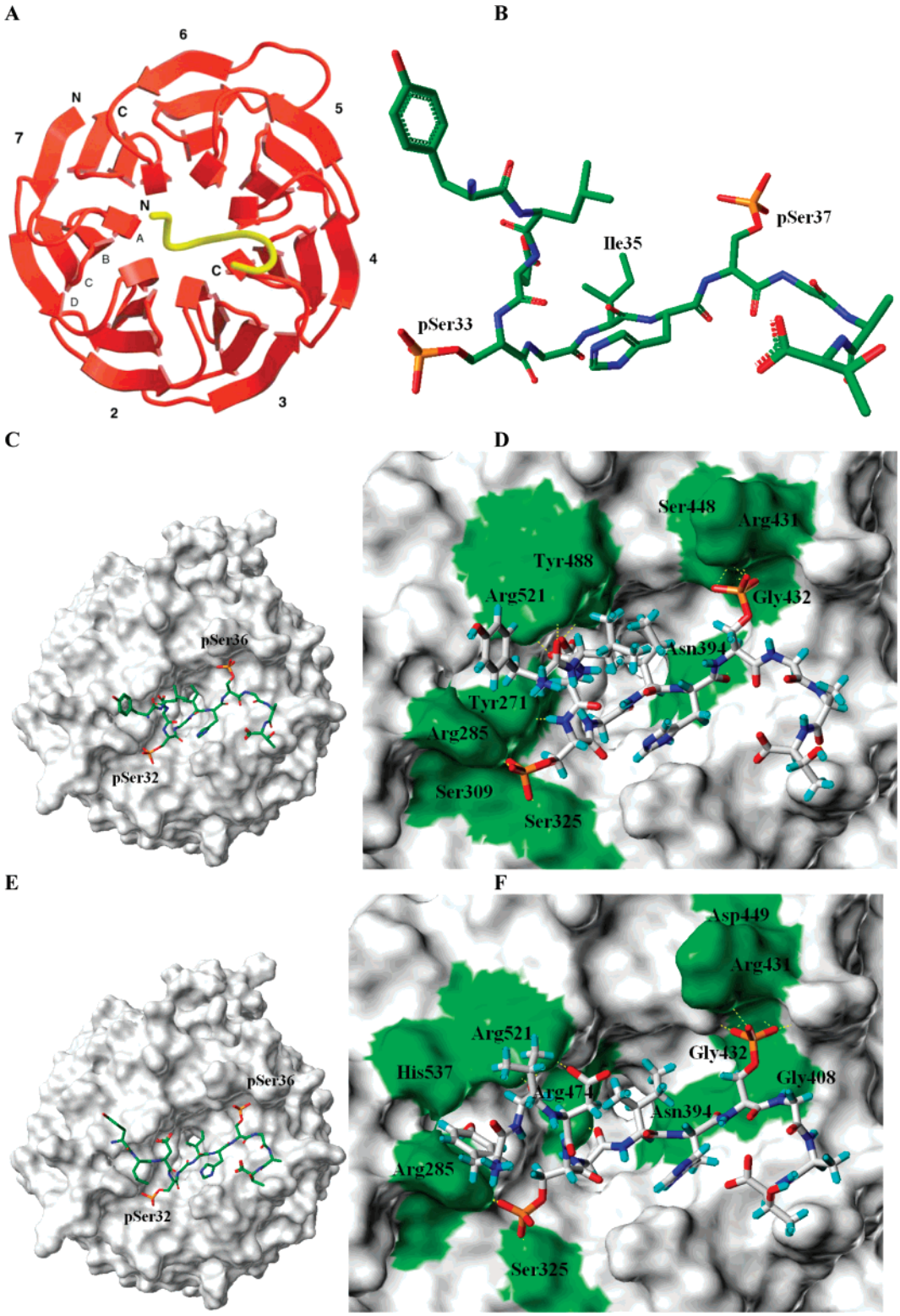

FIGURE 6: According to the crystal structure (*17*) of the human β-TrCP−Skp1 complex bound to a β-catenin peptide: (A) The phosphorylated β-catenin peptide binds to the top of the WD40 domain of β-TrCP, and it partially dips into the central channel. The seven blades of the WD40 domain are numbered from 1 to 7, and the strands within each blade are conventionally named A to D. (B) The diphosphorylated β-catenin YLD**pS**GIH**pS**GAT motif where both phosphate groups of **pSer** are shown, and point out of the structure bound to the β-TrCP protein. (C) Surface representation of the top face of the β-TrCP WD40 domain with the bound β-catenin peptide. (D) Close-up view of the interface between the β-TrCP WD40 domain and the doubly phosphorylated peptide ligand. (E and F) Results of docking studies starting with the crystal structure of the β-TrCP-Skp1 and the β-catenin peptide: (E) The β-TrCP is shown in surface representation. The β-catenin in stick format docks near the same amino acids in the interaction site on the surface than in the crystal structure. (F) Close-up view of the interface between the β-TrCP WD40 domain and the doubly phosphorylated peptide ligand, after docking. The β-catenin peptide binds to the top face of the β-TrCP WD40 domain. Asp^{32} makes contact with Tyr^{488} (W6); $pSer^{33}$ with Tyr^{271} (W1), Arg^{285} (W1), Ser^{309} (W2) and Ser^{325} (W2); and $pSer^{37}$ with Arg^{431} (W4−5), Gly^{432} (W5) and Ser^{448} (W5) of β-TrCP. Hydrogen bonds are represented by yellow dotted lines. Ile^{35} makes van der Waals contacts in the central channel.

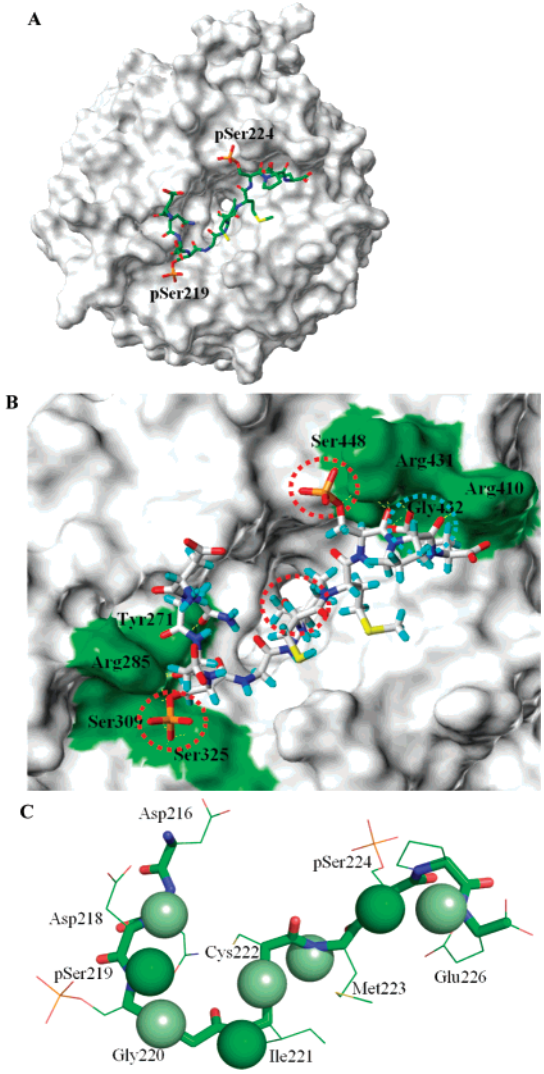

FIGURE 7: Results of docking studies starting with the NMR ATF4 bound structure. (A) The β-TrCP is shown in surface representation. After docking, ATF4 in ribbon format with acidic residues that are highlighted and labeled was found close to amino acids known to be in the interaction site on the surface. (B) Close-up view of the interface between the β-TrCP WD40 domain and the doubly phosphorylated peptide ligand: two interaction sites, Tyr^{271}, Arg^{285}, Ser^{309}, Ser^{325} and Arg^{410}, Arg^{431}, Gly^{432}, Ser^{448}, respectively are highlighted on the surface of the protein β-TrCP. 23P-ATF4 is in stick format in the interaction sites on the surface, with hydrogen bonds (in yellow dotted lines) between Asn^{217} and Tyr^{271} (W1), Asp^{218} and Arg^{285} (W1) and the first **pSer**^{219} residue with Arg^{285} (W1), Ser^{309} (W2) and Ser^{325} (W2), and the second **pSer**^{224} with Arg^{431} (W4−5). Interestingly, the Glu^{226} residues have the same interaction with Arg^{431} (W4−5), Gly^{432} (W5) and Ser^{448} (W5) as the second **pSer** of β-catenin. Ile^{221} with a position central in the D**pS**G**I**CM**pS** motif could reflect its particular role as in the study of the interaction of β-catenin with β-TrCP: Ile^{221} is able to make hydrophobic interactions with a hydrophobic pocket in the β-TrCP channel. These contacts could participate to increasing indirectly the affinity of the binding region. (C) Possible binding mode for 23P-ATF4 on the β-TrCP. The ATF4 structure after docking is shown in stick format with the side chains. Consistent with the net positive charge of the WD40 domain, interactions of ATF4 with β-TrCP are primarily made through its phosphate tails, **pSer**^{219}, **pSer**^{224}, and the negatively charged **Glu**^{226} side-chain, with β-TrCP Arg, Tyr and Ser residues, in addition to hydrophobic interaction between the Ile^{221} and the β-TrCP central channel. STD results have been added to the docked structure: the amide protons with the strongest STD amplification factor are displayed as colored spheres: green for the strongest, $Ileu^{221}$, **pSer**^{219} and **pSer**^{224}; light green for Asp^{218}, Gly^{220}, Cys^{222}, Met^{223} and Glu^{226}.

However, the motif region of the ATF4 peptide is modified upon docking, essentially the orientation of phosphorylated side chains (Figure 9), in order to accommodate ATF4 structure. The distance was measured between the phosphorus atoms of the two serines (Figure 9A), in the docked structure with an opposite orientation (17.8 Å) and in the NMR bound structure with a parallel orientation (11.1 Å). Because the distance between the two phosphate groups cannot be measured by NMR, this distant restraint was not incorporated for structure calculation. It can result in an incorrect orientation in the NMR bound structure, which is seen for the first phosphorylated **pSer**^{219} side chain (Figure 9A).

The STD-NMR results are also consistent with the conformational epitope obtained by docking (Figure 7C). The STD-NMR and the docking studies of the 23P-ATF4 in the presence of β-TrCP showed that nearly all the NH of the D**pS**G*XXX***pS** motif interact strongly with the corresponding amino acids inside the site. In addition, the side chain of the Glu^{226} residues is recognized. The charged phosphate groups are likely required, as several additional proton resonances giving rise to enhancements in the STD-NMR spectrum. The epitope comprises a surface extending over the E^{210}−N^{217} residues of 23P-ATF4, with contributions being made by side chain residues and by backbone residues. Ile^{221} whose hydrophobic nature is conserved in the peptide fragment could reflect its particular role in the D**pS**G**I**CM**pS** motif with its central position. STD-NMR data allowed determining which residues in addition to the D**pS**G*XXX***pS** β-TrCP recognition motif in ATF4 are important for interaction, such as the negatively charged ATF4 side chains D**pS**G**I***XX***pS***X***E**, particularly the **pSer**^{219}, **pSer**^{224} and the **Glu**^{226} residues. The fact that one Glu and one Asp were close to the **pSer** enhanced the negative potential generated by the phosphorylated Ser. This negative pole around the phosphate groups of the Ser reinforces the ATF4 binding to the β-TrCP protein. Indeed, a fragment composed of long negatively charged residues (**pSer** or Glu) and short Asp in close proximity was mainly indicated to interact with the β-TrCP protein. In the same way, a closely related, repeated sequence E**E**GFGSS**pS** (D/E and **pS**/E change) in human somatic Wee1 (*57*), important for its recognition and ubiquitination-dependent degradation by β-TrCP, may mimic the common binding motif, although one residue, **pSer**, is replaced by a Glu residue, and in E**E**G*XXXX***pS** the residue, **pSer**, is located two residues downstream of D**pS**G*XX***pS**.

Consequently docking against β-TrCP resulted in good predictions of the binding mode of ATF4. The derived structure−activity relationships by NMR together with the docking on the binding epitope may help to guide structure-assisted lead optimization in drug discovery. The binding motif is well conserved in ATF4 ligand identified to compete with another ligand to interact with the same WD repeat domain of β-TrCP, through an analogous phosphorylation motif.

3.2. Competition between Substrates for Binding to β-TrCP Revealed by STD-NMR on the Mixture of ATF4 and β-Catenin Peptides. The target-observed NMR titration method which combines STD-NMR with competition binding experiments useful under fast exchange conditions and for relatively weakly binding ligands allows the detection of the weak active site ligand, i.e., β-catenin, compared to

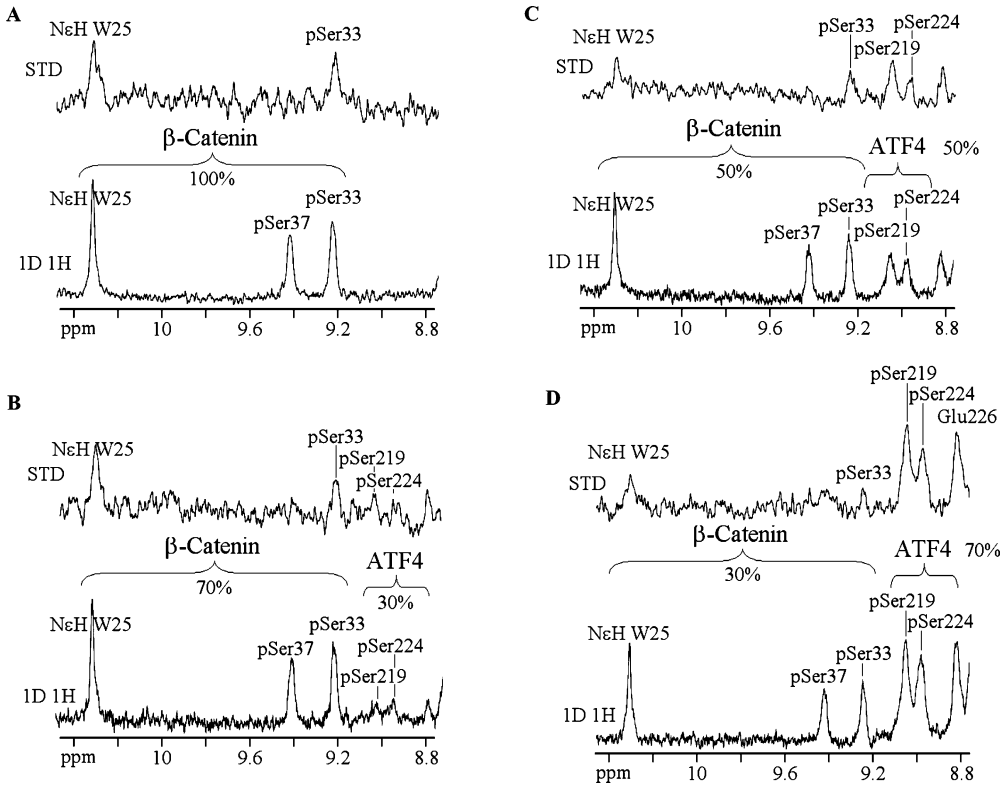

FIGURE 8: Competition STD-NMR. The 1D proton and STD-NMR spectra of 32P-β-catenin/β-TrCP upon addition of 23P-ATF4 illustrate the STD signal reduction of the indicator (32P-β-catenin) as a function of the competitor (23P-ATF4) concentration at different P-β-catenin:P-ATF4 ratios. (A) 1D proton spectrum of a weak ligand, 32P-β-catenin ($K_D \approx 1$ mM) used as an STD indicator at a concentration of 0.4 mM in the presence of 20 μM β-TrCP protein. Residues **pSer**^{33}, and the aromatic protons NϵH of Trp^{25} in close contact with β-TrCP protein, show positive peak in the corresponding STD-NMR spectrum. (B) The 1D proton and STD-NMR spectra of the same sample show that the STD signal intensities of 32P-β-catenin were reduced whereas the STD signal of the **pSer**^{219}, **pSer**^{224}, and Glu^{226}, amide signals of 23P-ATF4 at 9.05, 8.90 and 8.79 ppm, respectively were increased, upon addition of the 23P-ATF4 peptide (70:30). (C) Upon addition of the 23P-ATF4 peptide (50:50). (D) Upon addition of the 23P-ATF4 peptide (30:70).

the higher-affinity ligand, i.e., ATF4 (Figure 8). The ability to determine the binding affinity of inhibitors by the competition STD-NMR method leads to a rapid rank ordering of potential inhibitors that involves the evaluation of large numbers of analogues.

A great number of substrates of β-TrCP have been identified up to now. All share similar although not identical phosphorylation destruction motif compared to the canonical DSG*XX*S motif identified in the first known substrates of β-TrCP. All bind to the seven WD substrate binding domain of β-TrCP only if they are phosphorylated on the serine residues of this motif, with a more important role devoted to the first Ser residue. Thus a crucial question to understand the mechanism of action of β-TrCP and the importance of its functions in regulating numerous cellular pathways will be to determine whether and how all these substrates are able to compete between each other for binding to the same domain of β-TrCP. Understanding this will help considerably to modulate the activity of β-TrCP for therapeutic purposes against cancer and inflammation processes for example, while avoiding undesirable side effects due to other substrates. Toward this goal, we were able to analyze by STD-competition experiment the behavior of two different substrates with respect to β-TrCP when both simultaneously were present with the receptor E3 ligase protein. Thus, we could demonstrate for the first time that ATF4 was successfully competing with β-catenin for binding to β-TrCP. Hence, such STD-competition approach will pave the way to experimental design for modulating specifically a particular substrate of β-TrCP while avoiding to inhibit another nontargeted substrate.

3.3. Binding Comparison between the Two Competitors. We determined low energy docking sites for β-TrCP on stabilized structure of both β-catenin and ATF4 for a better understanding of the competition results. After the docking (Figure 7), the ATF4 peptide binds to the top face of the β-propeller, as in the X-ray complex (Figure 6A). We can generally assign three main common parts of the ATF4 peptide in contact with three β-TrCP binding pockets. The use of three regions of the WD domain for binding is similar to what has been observed in the binding of β-catenin, but with some differences.

In the first binding pocket, we found only the first phosphoserine of the β-catenin peptide in the X-ray complex (Figure 6D). The phosphate group pSer^{33} binds to a seven-bladed WD40 propeller domain (Figure 6D), forming two hydrogen bonds with Tyr^{271} and Arg^{285} (W1), and two others with Ser^{309} and Ser^{325} (W2); whereas three residues ND**pS** beginning the ATF4 motif occupy the same site of interaction (Figure 7B) with the β-TrCP protein (W1 and W2), creating a hydrogen bond network, which reinforces the interaction. The residue preceding the destruction motif, Asn^{217}, with its side chain makes a hydrogen bond with the hydroxyl group of Tyr271 (W1) of β-TrCP. The backbone carbonyl group of Asp^{218} makes intermolecular contact with Arg^{285} (W1). The phosphate group of **pSer**^{219} makes a charged-stabilized hydrogen bond with the hydroxyl groups of Ser^{309} and Ser^{325} (W2) and another hydrogen bond with Arg^{285} (W1).

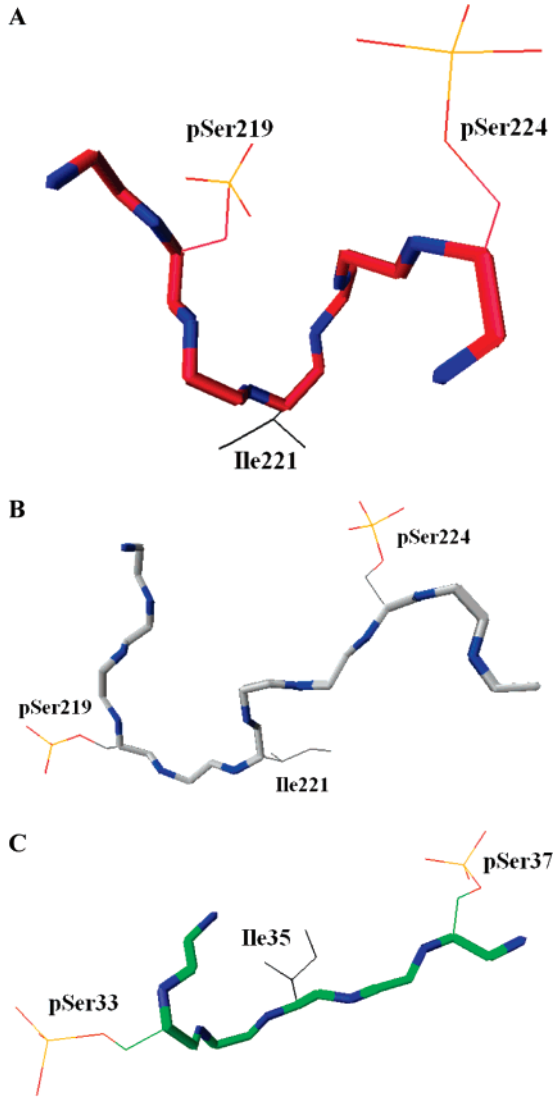

FIGURE 9: (A) The ATF4 motif D**pS**GI*XX***pS** in NMR low energy calculated structure forms a large bend with two opposite loops. This structure exposes the Ileu[221] in the center and the two phosphorylated **pSer**[219] and **pSer**[224] side chains implemented in the bend for interactions with the β-TrCP protein. (B) The DND**pS**GICM**pS**PE motif in docked ATF4 peptide structure. (C) The diphosphorylated β-catenin YLD**pS**GIH**pS**GAT motif.

The main structural changes between β-catenin and ATF4 reside in the second binding pocket. In β-catenin the second phosphoserine, **pSer**[37], is less implicated (Figure 8A), forming hydrogen bonds with Ser[448] (W5), Arg[431] (W4−5 linker) and Gly[432] (W5) (Figure 6E). The region after the DSG*XX*S motif is significantly less important for binding. On the other hand, three **pS**PE residues ending the motif of ATF4 are located at the W4−W5 position of the WD40 repeat motif (Figure 7C). The phosphate group of the second serine, **pSer**[224], forms hydrogen bonds and electrostatic interactions with the guanidium group of Arg[431] (W4−5 linker). Residue Pro[225] following the motif makes only one hydrogen bond, between the backbone carbonyl group of Pro[225] and the side chain of Arg[410] (W4), while Glu[226] makes much more extensive contacts. This is clearly important here to note that this Glu[226] residue was implicated in the same hydrogen bond network as the second phosphoserine, **pSer**[37] of the β-catenin (Figures 6 and 7). Its side chain makes a charged-stabilized hydrogen bond with Arg[431] (W4−5 linker) and two other hydrogen bonds with the backbone amide group of Gly[432] (W5), and the hydroxyl groups of Ser[448] (W5), which is in agreement with enhancements observed in the STD-NMR spectrum.

Finally, the third binding site appeared with the hydrophobic interaction between the Ile[221] of ATF4 peptide and the β-TrCP central channel, also involved with β-catenin (Figure 7C). The consensus motif in the β-catenin peptide has an extended conformation (Figure 9C), and we measured a large distance of 17.1 Å between the two phosphate groups. Despite an additional residue in the ATF4 motif, the distance between the two phosphate groups is also of 17.8 Å. The middle portion of the ATF4 peptide has an S-turn-like conformation (Figure 9B) that allows the side chain of Ile[221] to insert the farthest into the channel, as in the β-catenin−β-TrCP crystal structure, making intermolecular contacts. Ile[221] lies at the turning point between the two major ND**pS**, **pS**PE structure areas, thus dockings of the β-TrCP−phosphorylated ATF4 complex selected the exact positioning of the Ile[221] methyl tail dipping into the narrow central channel as a clip linkage leading to its stabilization. These similarities highlight the central channel as a structural scaffold that can adapt, through hydrophobic side chain, to recognizing diverse secondary structures and sequences. Consequently, in the consensus motif, the region containing the second phosphoserine is found to be different, which involves a large interatomic distance Ile[221]Cβ−**pSer**[224]P, 13.3 Å in the ATF4 docked structure and 8.9 Å in the β-catenin structure (Ile[35]Cβ−**pSer**[37]P). However, a similar distance, 10.1 Å, was found in the ATF4 docked structure by replacing **pSer**[224] by Glu[226] (Ile[221]Cβ−Glu[226]CO). We can observe that the interatomic distance implying the first phosphoserine was more similar: Ile[221]Cβ−**pSer**[219]P 9.5 Å in the docked structure and 10.4 Å in the β-catenin structure (Ile[35]Cβ−**pSer**[33]P).

These findings support the stucture-based conclusion that ND**pS**, **pS**PE and Ile[221] are critical for β-TrCP−ATF4 binding and specificity.

In conclusion, by determining conformations of ATF4, in interaction with β-TrCP at the molecular level compared with the interaction of β-catenin, we have established that structural differences in the amino acid sequence have an impact to identify key structural parts responsible for competitive inhibition. As the ATF4 inhibitor protein exerts a central role in cellular stress and inflammatory responses, the knowledge of its binding is a first important step toward the design of potent competitors that may have a therapeutic value.

ACKNOWLEDGMENT

We thank Geneviève Arnaud-Vincent (Centre for Technical Languages, Université Paris Descartes) for her critical reading of this manuscript.

SUPPORTING INFORMATION AVAILABLE

Tables listing some inter-residue ^{1}H−^{1}H distances from unambiguous NOE volumes and report rmsd statistics. Figures showing WaterLOGSY signal intensity as a function of the 23P-ATF4 ligand concentration, regions of the TRNOESY spectrum of 23P-ATF4 peptide in presence of MBP-β-TRCP, negative controls with reference 1D ^{1}H and

1D ^{1}H STD-NMR spectra and backbone dihedral Φ and Ψ angle rmsd values for 23P-ATF4 bound to β-TrCP protein. This material is available free of charge via the Internet at http://pubs.acs.org.

REFERENCES

1. Brindle, P. K., and Montminy, M. R. (1992) The CREB family of transcription activators, *Curr. Opin. Genet. Dev. 2*, 199−204.
2. Hai, T., Wolfgang, C. D., Marsee, D. K., Allen, A. E., and Sivaprasad, U. (1999) ATF3 and stress responses, *Gene Expression 7*, 321−335.
3. Oyadomari, S., Araki, E., and Mori, M. (2002) Endoplasmic reticulum stress-mediated apoptosis in pancreatic beta-cells, *Apoptosis 7*, 335−345.
4. Harding, H. P., Zhang, Y., Zeng, H., Novoa, I., Lu, P. D., Calfon, M., Sadri, N., Yun, C., Popko, B., Paules, R., Stojdl, D. F., Bell, J. C., Hettmann, T., Leiden, J. M., and Ron, D. (2003) An integrated stress response regulates amino acid metabolism and resistance to oxidative stress, *Mol. Cell 11*, 619−633.
5. Rutkowski, D. T., and Kaufman, R. J. (2003) All roads lead to ATF4, *Dev. Cell 4*, 442−444.
6. Lu, P. D., Harding, H. P., and Ron, D. (2004) Translation reinitiation at alternative open reading frames regulates gene expression in an integrated stress response, *J. Cell Biol. 167*, 27−33.
7. Vattem, K. M., and Wek, R. C. (2004) Reinitiation involving upstream ORFs regulates ATF4 mRNA translation in mammalian cells, *Proc. Natl. Acad. Sci. U.S.A. 101*, 11269−11274.
8. Tanaka, T., Tsujimura, T., Takeda, K., Sugihara, A., Maekawa, A., Terada, N., Yoshida, N., and Akira, S. (1998) Targeted disruption of ATF4 discloses its essential role in the formation of eye lens fibres, *Genes Cells 3*, 801−810.
9. Masuoka, H. C., and Townes, T. M. (2002) Targeted disruption of the activating transcription factor 4 gene results in severe fetal anemia in mice, *Blood 99*, 736−745.
10. Yang, X., Matsuda, K., Bialek, P., Jacquot, S., Masuoka, H. C., Schinke, T., Li, L., Brancorsini, S., Sassone-Corsi, P., Townes, T. M., Hanauer, A., and Karsenty, G. (2004) ATF4 is a substrate of RSK2 and an essential regulator of osteoblast biology; implication for Coffin-Lowry Syndrome, *Cell 117*, 387−398.
11. Elefteriou, F., Ahn, J. D., Takeda, S., Starbuck, M., Yang, X., Liu, X., Kondo, H., Richards, W. G., Bannon, T. W., Noda, M., Clement, K., Vaisse, C., and Karsenty, G. (2005) Leptin regulation of bone resorption by the sympathetic nervous system and CART, *Nature 434*, 514−520.
12. Chen, A., Muzzio, I. A., Malleret, G., Bartsch, D., Verbitsky, M., Pavlidis, P., Yonan, A. L., Vronskaya, S., Grody, M. B., Cepeda, I., Gilliam, T. C., and Kandel, E. R. (2003) Inducible enhancement of memory storage and synaptic plasticity in transgenic mice expressing an inhibitor of ATF4 (CREB-2) and C/EBP proteins, *Neuron 39*, 655−669.
13. Vallejo, M., Ron, D., Miller, C. P., and Habener, J. F. (1993) C/ATF, a member of the activating transcription factor family of DNA-binding proteins, dimerizes with CAAT/enhancer-binding proteins and directs their binding to cAMP response elements, *Proc. Natl. Acad. Sci. U.S.A. 90*, 4679−4683.
14. Liang, G., and Hai, T. (1997) Characterization of human activating transcription factor 4, a transcriptional activator that interacts with multiple domains of cAMP-responsive element-binding protein (CREB)-binding protein, *J. Biol. Chem. 272*, 24088−24095.
15. Gachon, F., Gaudray, G., Thebault, S., Basbous, J., Koffi, J. A., Devaux, C., and Mesnard, J. (2001) The cAMP response element binding protein-2 (CREB-2) can interact with the C/EBP-homologous protein (CHOP), *FEBS Lett. 502*, 57−62.
16. Lassot, I., Ségéral, E., Berlioz-Torrent, C., Durand, H., Groussin, L., Hai, T., Benarous, R., and Margottin-Goguet, F. (2001) ATF4 Degradation Relies on a Phosphorylation-Dependent Interaction with the SCFβ-TrCP Ubiquitin Ligase, *Mol. Cell. Biol. 21*, 2192−2202.
17. Wu, G., Xu, G., Schulman, B. A., Jeffrey, P. D., Harper, J. W., and Pavletich, N. P. (2003) Structure of a beta-TrCP1-Skp1-beta-catenin complex: destruction motif binding and lysine specificity of the SCF(beta-TrCP1) ubiquitin ligase, *Mol. Cell 11*, 1445−1456.
18. Coadou, G., Gharbi-Benarous, J., Megy, S., Bertho, G., Evrard-Todeschi, N., Segeral, E., Benarous, R., and Girault, J. P. (2003) NMR Studies of the Phosphorylation Motif of the HIV-1 Protein Vpu Bound to the F-Box Protein β-TrCP, *Biochemistry*, 14741−14751.
19. Megy, S., Bertho, G., Gharbi-Benarous, J., Baleux, F., Benarous, R., and Girault, J. P. (2005) STD and TRNOESY NMR Studies on the conformation of the oncogenic protein b-Catenin containing the phosphorylated motif DpSGXXpS bound to the b-TrCP protein., *J. Biol. Chem. 280*, 29107−29116.
20. Pons, J., Evrard-Todeschi, N., Bertho, G., Gharbi-Benarous, J., Sonois, V., Benarous, R., and Girault, J. P. (2007) Structural studies on 24P-IkBa peptide derived from a human IkB-a protein-related with the inhibition of the transcription factor nuclear NFkB activity, *Biochemistry 46*, 2958−2972.
21. Clore, G. M., and Gronenborn, A. M. (1982) Theory and Applications of the Transferred Nuclear Overhauser Effect to the Study of the Conformations of Small Ligands Bounds to Proteins, *J. Magn. Reson. 48*, 402−417.
22. Clore, G. M., and Gronenborn, A. M. (1983) Theory of the Time Dependent Transferred Nuclear Overhauser Effect: Applications to Structural Analysis of Ligand-Protein Complexes in Solution, *J. Magn. Reson. 53*, 423−442.
23. Klein, J., Meinecke, R., Mayer, M., and Meyer, B. (1999) Detecting binding affinity to immobilized receptor proteins in compound libraries by HR-MAS STD NMR, *J. Am. Chem. Soc. 121*, 5336−5337.
24. Mayer, M., and Meyer, B. (2001) Group epitope mapping by saturation transfer difference NMR to identify segments of a ligand in direct contact with a protein receptor, *J. Am. Chem. Soc. 123*, 6108−6117.
25. Mayer, M., and Meyer, B. (1999) Characterization of ligand binding by saturation transfer difference NMR spectroscopy, *Angew. Chem., Int. Ed. 38*, 1784−1788.
26. Shoichet, B. K., McGovern, S. L., Wei, B., and Irwin, J. J. (2002) Lead discovery using molecular docking, *Curr. Opin. Chem. Biol. 6*, 439−446.
27. Halperin, I., Ma, B., Wolfson, H., and Nussinov, R. (2002) Principles of docking: An overview of search algorithms and a guide to scoring functions, *Proteins 47*, 409−443.
28. Wang, Y. S., Liu, D., and Wyss, D. F. (2004) Competition STD NMR for the detection of high-affinity ligands and NMR-based screening, *Magn. Reson. Chem. 42*, 485−489.
29. Nallamsetty, S., Austin, B. P., Penrose, K. J., and Waugh, D. S. (2005) Gateway vectors for the production of combinatorially-tagged His6-MBP fusion proteins in the cytoplasm and periplasm of Escherichia coli, *Protein Sci. 14*, 2964−2971.
30. Marion, D., Ikura, M., Tschudin, R., and Bax, A. (1989) Rapid Recording of 2D NMR-Spectra without Phase Cycling—Application to the Study of Hydrogen-Exchange in Proteins, *J. Magn. Reson. 85*, 393−399.
31. Piotto, M., Saudek, V., and Sklenar, V. (1992) Gradient-tailored exitation for single-quantum NMR spectroscopy of aqueous solutions, *J. Biomol. NMR 2*, 661−665.
32. Hwang, T. L., and Shaka, A. J. (1995) Water Suppression That Works - Excitation Sculpting Using Arbitrary Wave-Forms and Pulsed-Field Gradients, *J. Magn. Reson. Ser. A 112*, 275−279.
33. Braunschweiler, L., and Ernst, R. R. (1983) Coherence transfer by isotropic mixing: application to proton correlation spectroscopy, *J. Magn. Reson. B 53*, 521−528.
34. Kumar, A., Ernst, R. R., and Wüthrich, K. (1980) A two-dimensional nuclear Overhauser enhancement (2D NOE) experiment for the elucidation of complete proton-proton cross-relaxation networks in biological macromolecules, *Biochem. Biophys. Res. Commun. 95*, 1−6.
35. Bothner-By, A. A., Stefens, R. L., Lee, J.-M., Arren, C. D., and Jeanloz, R. W. (1984) Structure determination of a tetrasaccharide: Transient nuclear Overhauser effects in the rotating frame, *J. Am. Chem. Soc. 106*, 811−814.
36. Bax, A., and Davis, D. G. (1985) MLEV-17-based two-dimensional homonuclear magnetization transfer spectroscopy, *J. Magn. Reson. 65*, 355−360.
37. Bodenhausen, G., and Ruben, D. J. (1980) Natural Abundance N-15 Nmr by Enhanced Heteronuclear Spectroscopy, *Chem. Phys. Let. 69*, 185−189.
38. Willker, W., Leibfritz, D., Kerssebaum, R., and Bermel, W. (1993) Gradient Selection in Inverse Heteronuclear Correlation Spectroscopy, *Magn. Reson. Chem. 31*, 287−292.
39. Bax, A., and Summers, M. F. (1986) 1H and 13C assignments from sensitivity-enhanced detection of heteronuclear multi-bond

connectivity by 2D multiple quantum NMR, *J. Am. Chem. Soc. 108*, 2093−2094.
40. Brünger, A. (1993) *X-PLOR manual*, Yale University Press, New Haven.
41. Dalvit, C., Fogliatto, G., Stewart, A., Veronesi, M., and Stockman, B. (2001) WaterLOGSY as a method for primary NMR screening: practical aspects and range of applicability, *J. Biomol. NMR 21*, 349−359.
42. Brünger, A. T., Adams, P. D., Clore, G. M., Gros, P., Grosse-Kunstleve, R. W., Jiang, J. S., Kuszewski, J., Nilges, M., Pannu, N. S., Read, R. J., Rice, L. M., Smonson, T., and Warren, G. L. (1998) Crystallography & NMR system (CNS): A new software system for macromolecular structure determination, *Acta Crystallogr. D54*, 905−921.
43. Linge, J. P., Habeck, M., Rieping, W., and Nilges, M. (2003) ARIA: automated assignment and NMR structure calculation, *Bioinformatics 19*, 315−316.
44. Schibli, D. J., Montelaro, R. C., and Vogel, H. J. (2001) The Membrane-Proximal Tryptophan-Rich Region of the HIV Glycoprotein, gp41, Forms a Well-Defined Helix in Dodecylphosphocholine Micelles, *Biochemistry 40*, 9570−9578.
45. Linge, J. P., O'Donoghue, S. I., and Nilges, M. (2001) Automated assignment of ambiguous nuclear overhauser effects with ARIA, *Methods Enzymol. 339*, 71−90.
46. Laskowski, R. A., Rullmann, J. A. C., MacArthur, M. W., Kaptein, R., and Thornton, J. M. (1996) AQUA and PROCHECK-NMR: programs for checking the quality of protein structures solved by NMR, *J. Biomol. NMR 8*, 477−486.
47. Koradi, R., Billeter, M., and Wüthrich, K. (1996) MOLMOL: a program for display and analysis of macromolecular structures, *J. Mol. Graphics 14*, 51−55.
48. Jain, A. N. (2003) Surflex: fully automatic flexible molecular docking using a molecular similarity-based search engine, *J. Med. Chem. 46*, 499−511.
49. Wüthrich, K. (1986) *NMR of Proteins and Nucleic Acids*, John Wiley & Sons, New York.
50. Vogtherr, M., and Peters, P. (2000) Application of NMR Based Binding Assays to Identify Key Hydroxy Groups for Intermolecular recognition, *J. Am. Chem. Soc. 122*, 6093−6099.
51. Meyer, B., and Peters, T. (2003) NMR spectroscopy techniques for screening and identifying ligand binding to protein receptors, *Angew. Chem., Int. Ed. 42*, 864−890.
52. Moller, H., Serttas, N., Paulsen, H., Burchell, J. M., Taylor-Papadimitriou, J., and Meyer, B. (2002) NMR-based determination of the binding epitope and conformational analysis of MUC-1 glycopeptides and peptides bound to the breast cancer-selective monoclonal antibody SM3, *Eur. J. Biochem. 269*, 1444−1455.
53. Kooistra, O., Herfurth, L., Luneberg, E., Frosch, M., Peters, T., and Zahringer, U. (2002) Epitope mapping of the O-chain polysaccharide of Legionella pneumophila serogroup 1 lipopolysaccharide by saturation-transfer-difference NMR spectroscopy, *Eur. J. Biochem. 269*, 573−582.
54. Johnson, M. A., Jaseja, M., Zou, W., Jennings, H. J., Copié, V., Pinto, B. M., and Pincus, S. H. (2003) NMR Studies of Carbohydrates and Carbohydrate-mimetic Peptides Recognized by an Anti-Group B *Streptococcus* Antibody, *J. Biol. Chem. 278*, 24740−24752.
55. Kumar, A., Wagner, G., Ernst, R. R., and Wüthrich, K. (1981) Buildup rates of the NOE measured by 2D Proton Magnetic Resonance Spectroscopy: Implication for studies of protein conformation, *J. Am. Chem. Soc. 103*, 3654−3658.
56. Vincent, S. J., Zwahlen, C., Post, C. B., Burgner, J. W., and Bodenhausen, G. (1997) The conformation of NAD+ bound to lactate dehydrogenase determined by nuclear magnetic resonance with suppression of spin diffusion, *Proc. Natl. Acad. Sci. U.S.A. 94*, 4383−4388.
57. Watanabe, N., Arai, H., Iwasaki, J., Shiina, M., Ogata, K., Hunter, T., and Osada, H. (2005) Cyclin-dependent kinase (CDK) phosphorylation destabilizes somatic Wee1 via multiple pathways, *Proc. Natl. Acad. Sci. U.S.A. 102*, 11663−11668.
58. Lassot, I., Estrabaud, E., Emiliani, S., Benkirane, M., Benarous, R., and Margottin-Goguet, F. (2005) p300 modulates ATF4 stability and transcriptional activity independently of its acetyltransferase domain, *J. Biol. Chem. 280*, 41537−41545.

BI7014212